In addition, the expression levels of the prosurvival proteins pCREB and BDNF also increased in *gad* mice. Consistent with these results, caspase-3 expression was suppressed in *gad* mice. Cryptorchid testes of *Uchl3* knockout mice showed slightly increased expression of the apoptotic proteins p53, Bax, and caspase-3 after injury, although similar increases were also observed in wild-type control mice. In total, these results suggest that UCH-L1 plays a role in balancing the expression of apoptosis-inducing and apoptosis-protecting proteins. In contrast, UCH-L3 seems to resist germ cell apoptosis after cryptorchid injury.

Recent studies demonstrate that many molecules in the cellular apoptosis machinery, such as p53,[39,41] Bcl-2 family,[42,43,54] XIAP,[52] and caspase[44] members, are targets for ubiquitination.[28] This suggests that ubiquitination is one of the major mechanisms by which apoptotic cell death is regulated. UCH-L1 has been suggested to associate with monoubiquitin,[13] and the monoubiquitin pool is reduced in *gad* mice relative to wild-type mice. Protection from cryptorchid injury was reported in testes of mice expressing a mutant K48R ubiquitin,[22] suggesting that ubiquitin plays a critical role in processing or modulating testicular insults. Normally, damaged proteins are polyubiquitinated and degraded via the ubiquitin-proteasome system; however, if damaged proteins are not degraded as easily when monoubiquitin is either depleted or mutated, then germ cell death could be delayed.[17,22] Our results with the *gad* mouse suggest that ubiquitin induction plays a critical role in regulating cell death during cryptorchid injury-mediated germ cell apoptosis.

*Uchl3* knockout mice exhibit severe retinal degeneration, suggesting that the UCH-L3-mediated ubiquitin pathway is involved in retinal homeostasis.[55] In the cryptorchid testes of *Uchl3* knockout mice, however, the profound testicular weight reduction and germ cell apoptosis after injury cannot be explained by ubiquitin induction alone. Our present results show that *Uchl3* knockout and wild-type mice have similar ubiquitin expression level in the testes, suggesting that UCH-L3 has another nonhydrolase activity in the ubiquitin-proteasome system. UCH-L3 also binds and cleaves the C-terminus of the ubiquitin-like protein, Nedd8.[14,56] This activity is unique to UCH-L3 because UCH-L1 does not cleave Nedd8. Thus, UCH-L3 appears to have dual affinities for ubiquitin and Nedd8. Our present results show that Nedd8 is strongly induced in scrotal testes of *Uchl3* knockout mice compared with those of wild-type mice (Figure 7). Cryptorchid testes of both *Uchl3* knockout and wild-type mice showed Nedd8 induction after injury, although the induction was higher in *Uchl3* knockout mice. These observations suggest that UCH-L3 may function as a deneddylating enzyme[16] *in vivo*, although further studies are necessary to clarify whether UCH-L3 interacts with Nedd8 during spermatogenesis.

In the present study, we demonstrate apparent reciprocal functions for the two deubiquitinating enzymes, UCH-L1 and UCH-L3, with respect to mediating injury after experimental cryptorchidism (Figure 8). Our results advance our understanding of the role of the ubiquitin-proteasome system in regulating apoptosis, and provide a unique opportunity for effective therapeutic intervention.

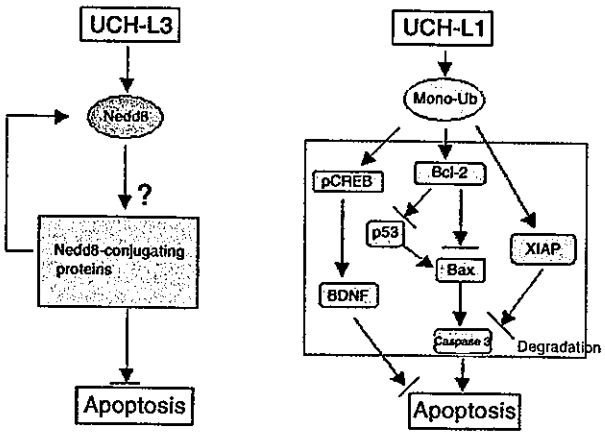


**Figure 8.** Differential function of the two UCH isozymes in response to experimental cryptorchidism. UCH-L3 has specificity for Nedd8. Cryptorchid injury results in protein damage and the accumulation of Nedd8-conjugated proteins. The accumulation of Nedd8-conjugated proteins in *Uchl3* knockout mice may contribute to profound germ cell loss via apoptosis. Hence, UCH-L3 might function as an anti-apoptotic regulator. UCH-L1 is involved in the maintenance of monoubiquitin levels. A deficiency in monoubiquitin results in delayed polyubiquitination and the accumulation of short-lived proteins after cryptorchid injury. Hence, UCH-L1 may function as a regulator of apoptosis.

## *Acknowledgments*

We thank Dr. S.M. Tilghman for providing *Uchl3* knockout mice, H. Kikuchi for technical assistance with tissue sections, and M. Shikama for the care and breeding of animals.

## *References*

1. Weissman AM: Themes and variations on ubiquitylation. Nat Rev Mol Cell Biol 2001, 2:169–178
2. Ciechanover A: The ubiquitin-proteasome pathway: on protein death and cell life. EMBO J 1998, 17:7151–7160
3. Pickart CM, Rose IA: Ubiquitin carboxyl-terminal hydrolase acts on ubiquitin carboxyl-terminal amides. J Biol Chem 1985, 260:7903–7910
4. Baker RT, Tobias JW, Varshavsky A: Ubiquitin-specific proteases of Saccharomyces cerevisiae. Cloning of UBP2 and UBP3, and functional analysis of the UBP gene family. J Biol Chem 1992, 267:23364–23375
5. Osawa Y, Wang YL, Osaka H, Aoki S, Wada K: Cloning, expression, and mapping of a mouse gene, Uchl4, highly homologous to human and mouse Uchl3. Biochem Biophys Res Commun 2001, 283:627–633
6. Kurihara LJ, Kikuchi T, Wada K, Tilghman SM: Loss of Uch-L1 and Uch-L3 leads to neurodegeneration, posterior paralysis and dysphagia. Hum Mol Genet 2001, 10:1963–1970
7. Kurihara LJ, Semenova E, Levorse JM, Tilghman SM: Expression and functional analysis of Uch-L3 during mouse development. Mol Cell Biol 2000, 20:2498–2504
8. Saigoh K, Wang YL, Suh JG, Yamanishi T, Sakai Y, Kiyosawa H, Harada T, Ichihara N, Wakana S, Kikuchi T, Wada K: Intragenic deletion in the gene encoding ubiquitin carboxy-terminal hydrolase in gad mice. Nat Genet 1999, 23:47–51
9. Kon Y, Endoh D, Iwanaga T: Expression of protein gene product 9.5, a neuronal ubiquitin C-terminal hydrolase, and its developing change in Sertoli cells of mouse testis. Mol Reprod Dev 1999, 54:333–341
10. Wilkinson KD, Deshpande S, Larsen CN: Comparisons of neuronal (PGP 9.5) and non-neuronal ubiquitin C-terminal hydrolases. Biochem Soc Trans 1992, 20:631–637
11. Liu Y, Fallon L, Lashuel HA, Liu Z, Lansbury Jr PT: The UCH-L1 gene

encodes two opposing enzymatic activities that affect alpha-synuclein degradation and Parkinson's disease susceptibility. Cell 2002, 111:209–218
12. Liu Y, Lashuel HA, Choi S, Xing X, Case A, Ni J, Yeh LA, Cuny GD, Stein RL, Lansbury Jr PT: Discovery of inhibitors that elucidate the role of UCH-L1 activity in the H1299 lung cancer cell line. Chem Biol 2003, 10:837–846
13. Osaka H, Wang YL, Takada K, Takizawa S, Setsuie R, Li H, Sato Y, Nishikawa K, Sun YJ, Sakurai M, Harada T, Hara Y, Kimura I, Chiba S, Namikawa K, Kiyama H, Noda M, Aoki S, Wada K: Ubiquitin carboxy-terminal hydrolase L1 binds to and stabilizes monoubiquitin in neuron. Hum Mol Genet 2003, 12:1945–1958
14. Wada H, Kito K, Caskey LS, Yeh ET, Kamitani T: Cleavage of the C-terminus of NEDD8 by UCH-L3. Biochem Biophys Res Commun 1998, 251:688–692
15. Hemelaar J, Borodovsky A, Kessler BM, Reverter D, Cook J, Kolli N, Gan-Erdene T, Wilkinson KD, Gill G, Lima CD, Ploegh HL, Ovaa H: Specific and covalent targeting of conjugating and deconjugating enzymes of ubiquitin-like proteins. Mol Cell Biol 2004, 24:84–95
16. Gong L, Kamitani T, Millas S, Yeh ET: Identification of a novel isopeptidase with dual specificity for ubiquitin- and NEDD8-conjugated proteins. J Biol Chem 2000, 275:14212–14216
17. Harada T, Harada C, Wang YL, Osaka H, Amanai K, Tanaka K, Takizawa S, Setsuie R, Sakurai M, Sato Y, Noda M, Wada K: Role of ubiquitin carboxy terminal hydrolase-L1 in neural cell apoptosis induced by ischemic retinal injury in vivo. Am J Pathol 2004, 164:59–64
18. Kwon J, Wang YL, Setsuie R, Sekiguchi S, Sakurai M, Sato Y, Lee WW, Ishii Y, Kyuwa S, Noda M, Wada K, Yoshikawa Y: Developmental regulation of ubiquitin C-terminal hydrolase isozyme expression during spermatogenesis in mice. Biol Reprod 2004, 71:515–521
19. Boekelheide K, Hall SJ: 2,5-Hexanedione exposure in the rat results in long-term testicular atrophy despite the presence of residual spermatogonia. J Androl 1991, 12:18–26
20. Ohta Y, Nishikawa A, Fukazawa Y, Urushitani H, Matsuzawa A, Nishina Y, Iguchi T: Apoptosis in adult mouse testis induced by experimental cryptorchidism. Acta Anat (Basel) 1996, 157:195–204
21. Yin Y, Hawkins KL, DeWolf WC, Morgentaler A: Heat stress causes testicular germ cell apoptosis in adult mice. J Androl 1997, 18:159–165
22. Rasoulpour RJ, Schoenfeld HA, Gray DA, Boekelheide K: Expression of a K48R mutant ubiquitin protects mouse testis from cryptorchid injury and aging. Am J Pathol 2003, 163:2595–2603
23. Yin Y, DeWolf WC, Morgentaler A: Experimental cryptorchidism induces testicular germ cell apoptosis by p53-dependent and -independent pathways in mice. Biol Reprod 1998, 58:492–496
24. Peltola V, Huhtaniemi I, Ahotupa M: Abdominal position of the rat testis is associated with high level of lipid peroxidation. Biol Reprod 1995, 53:1146–1150
25. Ahotupa M, Huhtaniemi I: Impaired detoxification of reactive oxygen and consequent oxidative stress in experimentally cryptorchid rat testis. Biol Reprod 1992, 46:1114–1118
26. Morimoto RI, Santoro MG: Stress-inducible responses and heat shock proteins: new pharmacologic targets for cytoprotection. Nature Biotechnol 1998, 16:833–838
27. Wojcik C: Proteasomes in apoptosis: villains or guardians? Cell Mol Life Sci 1999, 56:908–917
28. Yang Y, Yu X: Regulation of apoptosis: the ubiquitous way. EMBO J 2003, 17:790–799
29. Kwon J, Kikuchi T, Setsuie R, Ishii Y, Kyuwa S, Yoshikawa Y: Characterization of the testis in congenitally ubiquitin carboxy-terminal hydrolase-1 (Uch-L1) defective (gad) mice. Exp Anim 2003, 52:1–9
30. Taylor CT, Furuta GT, Synnestvedt K, Colgan SP: Phosphorylation-dependent targeting of cAMP response element binding protein to the ubiquitin/proteasome pathway in hypoxia. Proc Natl Acad Sci USA 2000, 97:12091–12096
31. Park C, Choi WS, Kwon H, Kwon YK: Temporal and spatial expression of neurotrophins and their receptors during male germ cell development. Mol Cells 2001, 12:360–367
32. Finkbeiner S: CREB couples neurotrophin signals to survival messages. Neuron 2000, 25:11–14
33. Selvakumaran M, Lin HK, Miyashita T, Wang HG, Krajewski S, Reed JC, Hoffman B, Liebermann D: Immediate early up-regulation of bax expression by p53 but not TGF beta 1: a paradigm for distinct apoptotic pathways. Oncogene 1994, 9:1791–1798
34. Liu L, Cavanaugh JE, Wang Y, Sakagami H, Mao Z, Xia Z: ERK5 activation of MEF2-mediated gene expression plays a critical role in BDNF-promoted survival of developing but not mature cortical neurons. Proc Natl Acad Sci USA 2003, 100:8532–8537
35. Matsui Y: Regulation of germ cell death in mammalian gonads. APMIS 1998, 106:142–148
36. Gosden R, Spears N: Programmed cell death in the reproductive system. Br Med Bull 1997, 53:644–661
37. Print CG, Loveland KL: Germ cell suicide: new insights into apoptosis during spermatogenesis. Bioessays 2000, 22:423–430
38. Lee JC, Peter ME: Regulation of apoptosis by ubiquitination. Immunol Rev 2003, 193:39–47
39. Haupt Y, Maya R, Kazaz A, Oren M: Mdm2 promotes the rapid degradation of p53. Nature 1997, 387:296–299
40. Oren M: Regulation of the p53 tumor suppressor protein. J Biol Chem 1999, 274:36031–36034
41. Ryan KM, Phillips AC, Vousden KH: Regulation and function of the p53 tumor suppressor protein. Curr Opin Cell Biol 2001, 13:332–337
42. Dimmeler S, Breitschopf K, Haendeler J, Zeiher AM: Dephosphorylation targets Bcl-2 for ubiquitin-dependent degradation: a link between the apoptosome and the proteasome pathway. J Exp Med 1999, 189:1815–1822
43. Marshansky V, Wang X, Bertrand R, Luo H, Duguid W, Chinnadurai G, Kanaan N, Vu MD, Wu J: Proteasomes modulate balance among proapoptotic and antiapoptotic Bcl-2 family members and compromise functioning of the electron transport chain in leukemic cells. J Immunol 2001, 166:3130–3142
44. Suzuki Y, Nakabayashi Y, Takahashi R: Ubiquitin-protein ligase activity of X-linked inhibitor of apoptosis protein promotes proteasomal degradation of caspase-3 and enhances its anti-apoptotic effect in Fas-induced cell death. Proc Natl Acad Sci USA 2001, 98:8662–8667
45. Yin Y, Stahl BC, DeWolf WC, Morgentaler A: P53 and Fas are sequential mechanisms of testicular germ cell apoptosis. J Androl 2002, 23:64–70
46. Ohta H, Aizawa S, Nishimune Y: Functional analysis of the p53 gene in apoptosis induced by heat stress or loss of stem cell factor signaling in mouse male germ cells. Biol Reprod 2003, 68:2249–2254
47. Beumer TL, Roepers-Gajadien HL, Gademan IS, Lock TM, Kal HB, De Rooij DG: Apoptosis regulation in the testis: involvement of Bcl-2 family members. Mol Reprod Dev 2000, 56:353–359
48. Oldereid NB, Angelis PD, Wiger R, Clausen OP: Expression of Bcl-2 family proteins and spontaneous apoptosis in normal human testis. Mol Hum Reprod 2001, 7:403–408
49. Borner C: The Bcl-2 protein family: sensors and checkpoints for life-or-death decisions. Mol Immunol 2003, 39:615–647
50. Yamamoto CM, Sinha Hikim AP, Huynh PN, Shapiro B, Lue Y, Salameh WA, Wang C, Swerdloff RS: Redistribution of Bax is an early step in an apoptotic pathway leading to germ cell death in rats, triggered by mild testicular hyperthermia. Biol Reprod 2000, 63:1683–1690
51. Deveraux QL, Reed JC: IAP family proteins—suppressors of apoptosis. Genes Dev 1999, 13:239–252
52. Yang Y, Fang S, Jensen JP, Weissman AM, Ashwell JD: Ubiquitin protein ligase activity of IAPs and their degradation in proteasomes in response to apoptotic stimuli. Science 2000, 288:874–877
53. Deveraux QL, Roy N, Stennicke HR, Van Arsdale T, Zhou Q, Srinivasula SM, Alnemri ES, Salvesen GS, Reed JC: IAPs block apoptotic events induced by caspase-8 and cytochrome c by direct inhibition of distinct caspases. EMBO J 1998, 17:2215–2223
54. Li B, Dou QP: Bax degradation by the ubiquitin/proteasome-dependent pathway: involvement in tumor survival and progression. Proc Natl Acad Sci USA 2000, 97:3850–3855
55. Semenova E, Wang X, Jablonski MM, Levorse J, Tilghman SM: An engineered 800 kilobase deletion of Uchl3 and Lmo7 on mouse chromosome 14 causes defects in viability, postnatal growth and degeneration of muscle and retina. Hum Mol Genet 2003, 12:1301–1312
56. Dil Kuazi A, Kito K, Abe Y, Shin RW, Kamitani T, Ueda N: NEDD8 protein is involved in ubiquitinated inclusion bodies. J Pathol 2003, 199:259–266

Available online at www.sciencedirect.com
SCIENCE DIRECT
Neuroscience Letters 374 (2005) 98–103
Neuroscience Letters
www.elsevier.com/locate/neulet

# Mitochondrial localization of cellular prion protein ($PrP^C$) invokes neuronal apoptosis in aged transgenic mice overexpressing $PrP^C$

Naomi S. Hachiya[a,b], Makiko Yamada[a,b], Kota Watanabe[a,b], Akiko Jozuka[a,b], Takuya Ohkubo[a,c], Kenichi Sano[a,1], Yoshio Takeuchi[a,2], Yoshimichi Kozuka[d], Yuji Sakasegawa[a], Kiyotoshi Kaneko[a,b,*]

[a] *Departments of a Cortical Function Disorders, National Institute of Neuroscience (NIN), National Center of Neurology and Psychiatry (NCNP), Kodaira, Tokyo 187-8502, Japan*
[b] *Core Research for Evolutional Science and Technology (CREST), Japan Science and Technology Agency, Kawaguchi, Saitama 332-0012, Japan*
[c] *Department of Neurology and Neurological Science, Graduate School of Medicine, Tokyo Medical and Dental University, Bunkyo-ku, Tokyo 113-0034, Japan*
[d] *Ultrastructural Research, National Institute of Neuroscience (NIN), National Center of Neurology and Psychiatry (NCNP), Kodaira, Tokyo 187-8502, Japan*

Received 14 September 2004; received in revised form 12 October 2004; accepted 13 October 2004

**Abstract**

Recent studies suggest that the disease isoform of prion protein ($PrP^{Sc}$) is non-neurotoxic in the absence of cellular isoform of prion protein ($PrP^C$), indicating that $PrP^C$ may participate directly in the neurodegenerative damage by itself. Meanwhile, transgenic mice harboring a high-copy-number of wild-type mouse (Mo) $PrP^C$ develop a spontaneous neurological dysfunction in an age-dependent manner, even without inoculation of $PrP^{Sc}$ and thus, investigations of these aged transgenic mice may lead to the understanding how $PrP^C$ participate in the neurotoxic property of PrP. Here we demonstrate mitochondria-mediated neuronal apoptosis in aged transgenic mice overexpressing wild-type $MoPrP^C$ (Tg(MoPrP)4053/FVB). The aged mice exhibited an aberrant mitochondrial localization of $PrP^C$ concomitant with decreased proteasomal activity, while younger littermates did not. Such aberrant mitochondrial localization was accompanied by decreased mitochondrial manganese superoxide dismutase (Mn-SOD) activity, cytochrome *c* release into the cytosol, caspase-3 activation, and DNA fragmentation, most predominantly in hippocampal neuronal cells. Following cell culture studies confirmed that decrease in the proteasomal activity is fundamental for the $PrP^C$-related, mitochondria-mediated apoptosis. Hence, the neurotoxic property of $PrP^C$ could be explained by the mitochondria-mediated neuronal apoptosis, at least in part.


*Keywords:* $PrP^C$; Proteasomal activity; Mitochondrial localization; Superoxide dismutase activity; Mitochondria-mediated apoptosis

The posttranslational conformational change of the cellular isoform of prion protein ($PrP^C$) into its scrapie isoform ($PrP^{Sc}$) is the fundamental process underlying the pathogenesis of prion diseases [24], but the molecular events through which prion infection and the resulting accumulation of PrP lead to the neuronal dysfunction, vacuolation, and death that characterize prion pathology remain unclear [6].

Importantly, $PrP^{Sc}$, the disease isoform of PrP, seems to be non-neurotoxic in the absence of $PrP^C$, suggesting that $PrP^C$ may participate directly in the prion neurodegenerative damage by itself, and the cellular pathways activated by neurotoxic forms of PrP that ultimately result in neuronal death are also being investigated, and several possible mechanisms have been uncovered [6]. For example, cross-linking

* Corresponding author. Tel.: +81 42 346 1718; fax: +81 42 346 1748.
*E-mail address:* kaneko@ncnp.go.jp (K. Kaneko).
[1] Present address: Hinoieda Kagaku Ltd., Hino-city, Tokyo 191-0061, Japan.
[2] Present address: KOHJIN-BIO Ltd., Sakado-city, Saitama 350-0214, Japan.

0304-3940/$ – see front matter © 2004 Elsevier Ireland Ltd. All rights reserved.
doi:10.1016/j.neulet.2004.10.044

$PrP^C$ in vivo with specific monoclonal antibodies was found to trigger neuronal apoptosis, suggesting that $PrP^C$ functions in the control of neuronal survival [26]. In fact, neural tissues overexpressing $PrP^C$ grafted into the brains of $PrP^C$-deficient mice develop the severe histopathological changes characteristic of prion disease when infected with prions, but no pathological changes were seen in $PrP^C$-deficient tissue, not even in the immediate vicinity of the grafts despite the presence of high levels of $PrP^{Sc}$ [2]. In addition, interruption of $PrP^C$ expression during an ongoing prion infection prevents neuronal loss and reverses early spongiform change [16]. The continued accumulation of $PrP^{Sc}$ in this model after neuronal $PrP^C$ depletion is likely to reflect prion replication predominantly in both microglia and astrocytes glial cells without $PrP^C$ depletion, which support $PrP^{Sc}$ replication. The $PrP^{Sc}$ deposits colocalize with astrocytes in the brains of infected mice with neuronal $PrP^C$ depletion, which was not seen in scrapie-infected control animals without PrP depletion. The fact that these mice remain asymptomatic indicates that even extensive extraneuronal $PrP^{Sc}$ replication does not cause clinical disease or neurodegeneration in this model. Thus, neuronal $PrP^C$ seems to be fundamental for the neurotoxic property of PrP even in the $PrP^{Sc}$-infected conditions, but the detailed molecular events especially with non-mutant, wild-type $PrP^C$ still remained unclear.

Meanwhile, aged transgenic mice harboring a high-copy-number of wild-type PrP-B transgenes spontaneously developed mitochondrial encephalomyopathy including focal vacuolation of the central nervous system, skeletal muscles and peripheral nerves without $PrP^{Sc}$ inoculation [28]. Such focal vacuolation was localized to the hippocampus, the superior colliculus, and midbrain tegmentum, which resembled that seen in experimental scrapie, albeit less intense. Other transgenic lines harboring a high-copy-number of wild-type PrP transgenes also exhibited spontaneous neurological dysfunction in an age-dependent manner [21,27]. For example, transgenic mice overexpressing the wild-type mouse (Mo) PrP-A gene (Tg(MoPrP)4053/FVB) used in this study became symptomatic at around the age of 700 days, although no pathological evidence for prion diseases was evident [27]. Since no $PrP^{Sc}$ has been inoculated in these mice, investigations of these aged transgenic mice overexpressing wild-type $PrP^C$ may lead to the better understanding how $PrP^C$ participate in the neurotoxic property of PrP.

Here we show that the Tg(MoPrP)4053/FVB mice exhibited an aberrant mitochondrial localization of $PrP^C$ accompanied by decreased mitochondrial manganese superoxide dismutase (Mn-SOD) activity, cytochrome *c* release in the cytosol, caspase-3 activation, and DNA fragmentation, concomitant with decreased proteasomal activity in an age-dependent manner.

Tg(MoPrP)4053/FVB and its littermate were kindly provided by Dr. S.B. Prusiner (University of California, San Francisco). Antibodies K3 and K4 against PrP were rabbit polyclonal sera raised against PrP peptides corresponding to residues 76–90 and 96–110 in MoPrP, respectively. Anti-cytochrome *c* and anti-porin antibodies were purchased from BD Biosciences. Anti-Hsc70 antibody was purchased from Stressgen Biotechnologies Corporation. Mitotracker Red CMXRos was purchased from Molecular Probes. Lactacystin, ALLN, and MG132 were purchased from Sigma. The $\Delta\Psi m$ detection kit and APO-BrdU TUNEL assay kit were purchased from Trevigen Inc. and Molecular Probes, respectively. Antibodies were used at 1:1000 (Western blotting) or 1:100 (immunofluorescence microscopy) unless otherwise noted. For immuno-electronmicroscopy, 10 nm golds were purchased from DAKO.

Cells or brains were homogenized with 9 volumes of mitochondrial buffer (220 mM mannitol, 70 mM sucrose, 10 mM Hepes-KOH, pH 7.4, and 0.1 mM EDTA) and centrifuged at $700 \times g$ for 5 min at 4 °C, and the supernatant was further centrifuged at $5000 \times g$ for 10 min at 4 °C. The supernatant was used as a post-mitochondrial supernatant. The resulted pellet was washed three times with mitochondrial buffer, resuspended in 9 volumes of the same buffer, and then centrifuged at $2000 \times g$ for 2 min at 4 °C followed by $5000 \times g$ for 8 min at 4 °C. The pellet was resuspended in 9 volumes of the same buffer, and then centrifuged at $5000 \times g$ for 10 min at 4 °C. The final pellet was recovered and stored on ice until use (mitochondrial fraction). The post-mitochondrial supernatant was further centrifuged at $100{,}000 \times g$ for 1 h at 4 °C, and the supernatant was used as cytosolic fraction, and the pellet was resuspended in mitochondrial buffer (microsome fraction). Western blots were performed at 5 μg of total protein/lane.

Mitochondrial manganese superoxide dismutase (Mn-SOD) and cytosolic copper/zinc SOD (Cu/Zinc-SOD) activities were measured by the SOD assay kit (Dojindo Molecular Technologies, Inc.), and cytosolic glutathione (GSH) was measured by the Glutathione quantification kit (Dojindo Molecular Technologies, Inc.) according to the manufacturer's instructions. Caspase-3 activity was measured using the PARP Western Blot Kit (WAKO) according to the manufacturer's instructions. DNA fragmentation was measured by the TUNEL assay (ApopTag® Peroxidase *In situ* Apoptosis Detection Kit, CHEMICON International), which was performed according to the manufacturer's instructions before being visualized with an Olympus CX40 (Olympus Optical Co., Ltd.). Sections were counter-stained by 0.5% methyl green (WAKO) in 0.1 M sodium acetate (pH 4.0).

Proteasomal activity assay was performed as previously described [3,9,31].

Tg(MoPrP)4053/FVB harboring a high-copy-number of wild-type PrP-A transgenes at the age of 520 days (TG520) and an age-matched non-transgenic littermate (WT520) showed similar migration rates of $PrP^C$ on poly acrylamide gel electrophoresis and Western blotting using anti-PrP-antibody K4 (Fig. 1A, PK(−)). As increased resistance to protease K digestion is often a feature of $PrP^{Sc}$, this was examined in TG520 and WT520. No resistance to proteinase K digestion was detected in any of these mice (Fig. 1A, PK(+)). Histological examinations of the TG520 brains including

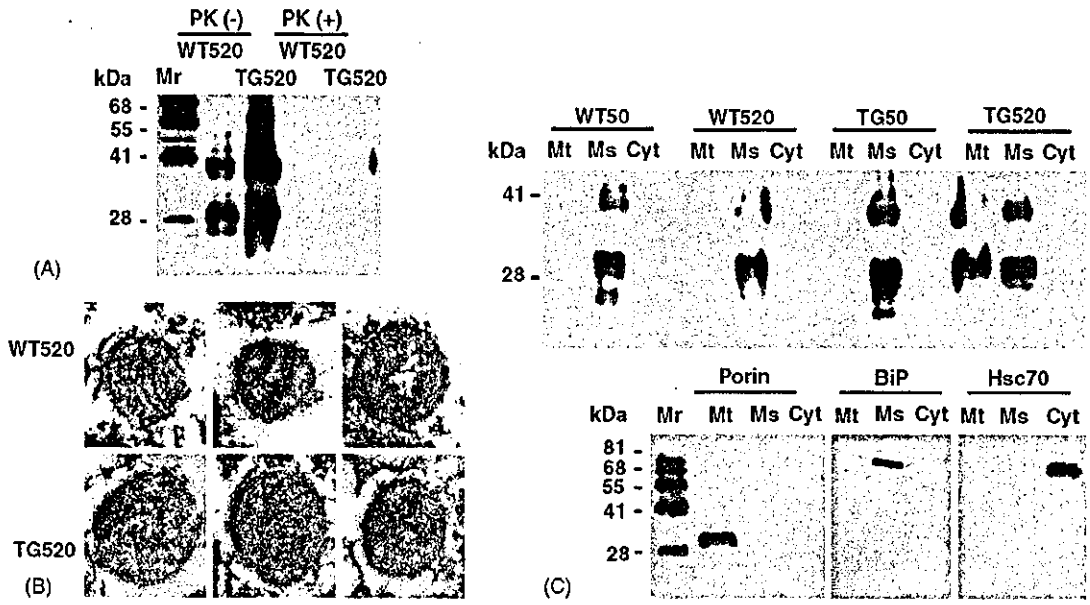


Fig. 1. $PrP^C$ is localized to the mitochondrial fraction in Tg(MoPrP)4053/FVB overexpressing wild-type $PrP^C$. WT520: non-transgenic littermate at the age of 520 days. TG520: Tg(MoPrP)4053/FVB at the age of 520 days. WT50: non-transgenic littermate at the age of 50 days. TG50: Tg(MoPrP)4053/FVB at the age of 50 days. (A) Western blot analysis and resistance to proteinase K digestion of $PrP^C$ in WT520 and TG520. PK(−): Western blot analysis with anti-PrP antibody K4. Bands derived from $PrP^C$ appear to be normal. PK(+): resistance to proteinase K digestion. Five hundred microliter of brain homogenates (5 μg of total protein/lane) were digested with proteinase K (20 μg/ml, Sigma) at 37 °C for 1 h followed by centrifugation at 100,000 × *g* for 1 h at 4 °C and the resuspended pellet was loaded onto the gels. No resistance to proteinase K digestion is detected. Mr: molecular weight marker. (B) Immuno electron microscopy (30,000×) detects $PrP^C$ with anti-PrP K3 (10 nm golds) in the mitochondria of neuronal cells in TG520. (C) Total brain homogenates of TG520 exhibit aberrant localization of overexpressed $PrP^C$, whereas those of WT50, WT520 and TG50 do not. Western blot analysis with anti-PrP antibody K4 (1:1000). Anti-porin antibody (1:1000) was used as a mitochondrial (Mt) marker, anti-BiP antibody (1:1000) was used as a microsome (Ms) marker, and anti-Hsc70 antibody (1:1000) was used as a cytosolic (Cyt) marker.

dentate gyrus, hippocampus, other cerebral cortices, basal ganglia and cerebellum by hematoxylin and eosin as well as methyl green-pyronin staining revealed no apparent pathological evidence in the brain sections of WT520 and TG520 (data not shown).

Since older transgenic mice (not inoculated with $PrP^{Sc}$) that harbor a high-copy-number of wild-type PrP-B transgenes develop mitochondrial encephalomyopathy including focal vacuolation of the central nervous system, skeletal muscles and peripheral nerves [28], we set out to determine whether $PrP^C$ could be detected in the mitochondrial fraction of TG520. Although the TG520 appeared clinically and histologically normal, they exhibited aberrant mitochondrial localization of $PrP^C$ as determined by immuno electron microscopy; immunogold-labelled $PrP^C$ localized at the mitochondria of the granular cells in the hippocampal dentate gyrus of TG520 but not of WT520 (Fig. 1B). Such aberrant mitochondrial localization of $PrP^C$ was further confirmed in TG520 by Western blotting using a subcellular fractionation, whereas younger non-transgenic littermate at the age of 50 days (WT50), WT520, and younger Tg(MoPrP)4053/FVB at the age of 50 days (TG50) did not exhibit the feature (Fig. 1C).

The oxidative stress leads to dysfunctions of the respiratory enzymes and the depletion of ATP followed by a decrease in reduced glutathione (GSH) concentration, which triggers the cycle of oxidative stress, mitochondrial dysfunction, and further antioxidant depletion. Exposure of tissue to oxygen free radicals results in lipid peroxidation, protein oxidation and DNA damage, which is in concert with "apoptosis". In order to prevent such damages, mammalian cells are equipped with both non-enzymatic and enzymatic scavenging systems to eliminate oxygen free radicals, anti oxidant enzymes, i.e., SOD, catalase, and glutathione peroxidase are essential to cells in removing $O_2^-$ and hydrogen peroxide ($H_2O_2$) from the tissues exposed to oxidative stress. Therefore, we next examined mitochondrial Mn-SOD as well as cytosolic Cu/Zn-SOD activities.

The mitochondrial Mn-SOD activity decreased significantly in TG520 compared to that in WT50, TG50, or WT520 (Fig. 2A), whereas no significant difference in the cytosolic copper/zinc SOD (Cu/Zn-SOD) activity was observed among them (Fig. 2B). Furthermore, cytosolic GSH level was dramatically decreased in TG520 but not in WT50, TG50, or WT520 (Fig. 2C). These results indicated that mitochondria-localized $PrP^C$ induced oxidative stress in TG520.

Subsequently, release of cytochrome *c* from the inner-membrane space into the cytosol (Fig. 3A), caspase-3 activation (Fig. 3B), and DNA fragmentation (Fig. 3C) were observed in TG520 brain, whereas no release of cytochrome *c*/ DNA fragmentation but faint caspase-3 activation was detected in WT520 brain (Fig. 3A–C). Serial specimens of TG520 and WT520 brains were further examined by

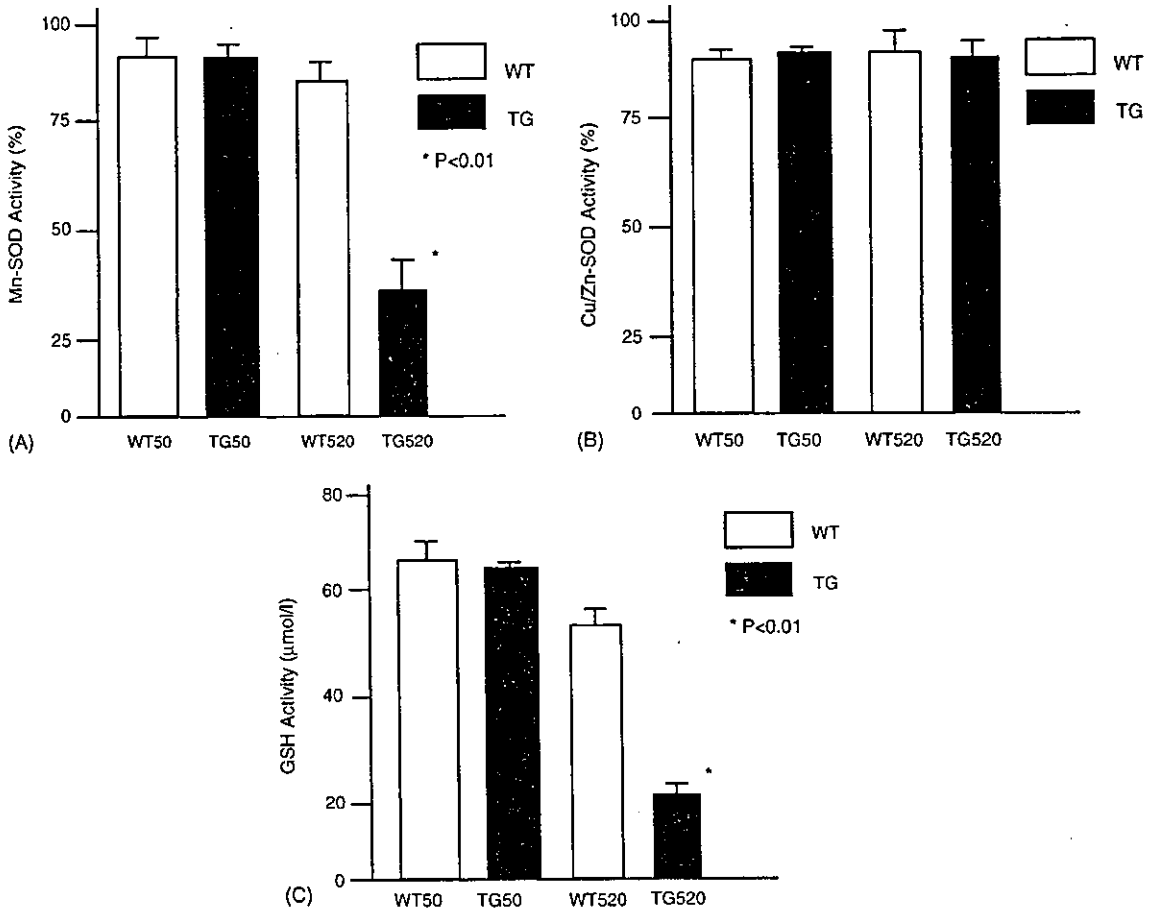


Fig. 2. Mitochondria-localized $PrP^C$ induces oxidative stress in TG520. (A) Mitochondrial manganese superoxide dismutase (Mn-SOD) and (B) cytosolic copper/zinc SOD (Cu/Zinc-SOD) activities. The Mn-SOD activity decreases significantly in TG520 compared to that in WT50, TG50 or WT520, whereas the cytosolic Cu/Zn-SOD activity remained similar among them. Error bars represent mean ± S.D. (C) Cytosolic glutathione (GSH) level is dramatically decreased in TG520 but not in WT50, TG50, or WT520. Error bars represent mean ± S.D.

the TUNEL assay (Fig. 3D). As shown, the TUNEL assay showed that the DNA fragmentation most predominantly in granular cells in the hippocampal dentate gyrus and to a lesser extent pyramidal cells in the CA1 and CA2 regions of TG520 (Fig. 3D).

In an age-dependent development of other aggregation disorders, the accumulation and aggregation of the disease related-proteins are associated with an age-dependent decrease in proteasomal activity and are promoted by inhibition of proteasomal activity [31]. Therefore, it is also likely that such aberrant mitochondrial localization requires $PrP^C$ retained in the cytoplasm with the proteasomal activity decreased. Therefore, the hydrolysis of Suc-Leu-Leu-Val-Tyr-4-methyl-coumaryl-7-amide (Suc-LLVY-MCA) by chymotrypsin-like proteasomal activity in brain homogenates of WT50, WT520, TG50, and TG520 was then investigated. As expected, proteasomal activity of both transgenic mice Tg(MoPrP)4053/FVB and non-transgenic littermate decreased with increasing age (Fig. 3E).

The posttranslational conformational change of $PrP^C$ into $PrP^{Sc}$ is the fundamental process underlying the pathogenesis of prion diseases [24]. Many concurrent reports have suggested that $PrP^C$ may play a role in neuronal survival or death. The removal of serum from cells in culture causes apoptosis in $PrP^C$-deleted cells but not in wild-type cells [13]. $PrP^C$ also inhibits Bax-mediated neuronal apoptosis in human primary neurons [1]. The binding of a ligand to $PrP^C$ transduces neuroprotective signaling through a cAMP/PKA-dependent pathway. Therefore, $PrP^C$ may function as a trophic receptor whose activation results in a neuroprotective state [5].

On the other hand, misfolded $PrP^C$ is subject to degradation by proteasomes. Like many misfolded secretory proteins [12,23], it is recognized in the ER and subject to retrograde transport to the cytoplasm and degradation by the proteasome [11,14,29,30]. Or, a small fraction of PrP chains is not translocated into the ER lumen during synthesis, and is rapidly degraded in the cytoplasm by the proteasome as far as proteasome function remains normal [8]. As proteasome function gradually decreases with age over a very long period or with inhibitors in the case of cultured cells, $PrP^C$ overflows in the cytoplasm, targeted to the mitochondria, which subsequently induces the mitochondria-mediated apoptosis.

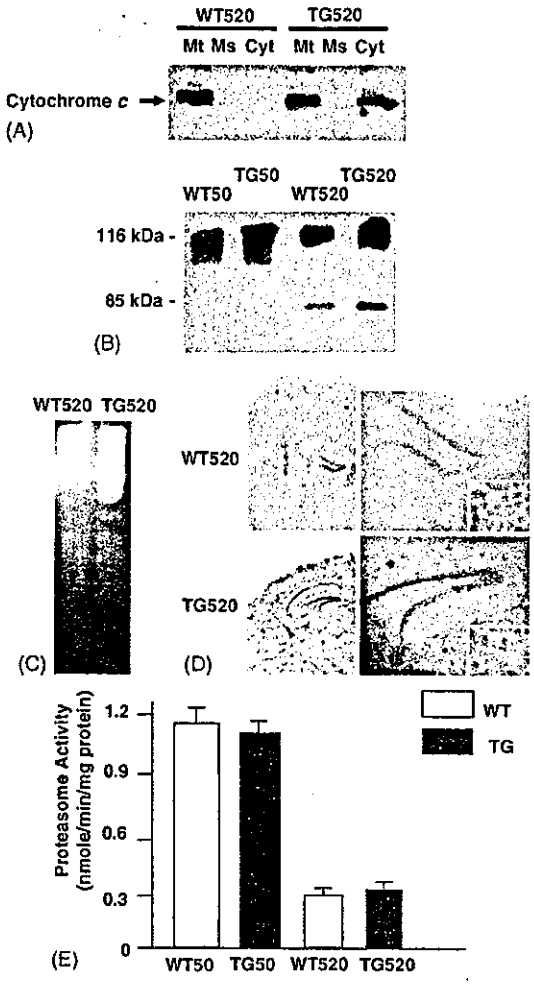


Fig. 3. Neuronal apoptosis in the TG520 brain. (A) Measurement of cytochrome *c* released into the cytosol. Western blot analysis with anti-cytochrome *c* antibody detects cytochrome *c* in the cytosol of the TG520 but not WT520 brain. Mt: mitochondrial fraction, Ms: microsome fraction, Cyt: cytosolic fraction. (B) Caspase-3 activation in TG520 brain. Brain homogenates (5 μg of total protein/lane) of younger WT50 and TG50 do not exhibit caspase-3 activation. Note that a faint band is detected in WT520 brain. The 85 kDa bands corresponding to the degradation products of poly ADP-ribose polymerase (PARP, 116 kDa) is a measure of caspase-3 activity. (C) DNA fragmentation in brain homogenates of TG520 is shown (1 μg of genomic DNA/lane). Brain homogenates of WT520 show no DNA fragmentation. Genomic DNAs were applied onto 1% agarose gel. (D) Serial frozen sections of total brains (left panels) and the hippocampal regions (right panels, 40×, lower right corner panels, 400×) were made. Top panels: WT520. Bottom panels: TG520. Neuronal apoptosis (brown) is evident in the bottom panels as compared with the top panels. (E) Age-dependent decrease in brain proteasomal activity. Chymotrypsin-like proteolytic activity was assayed in brain homogenates (1 μg of total protein/assay) of WT50, TG50, WT520, and TG520. Error bars represent mean ± S.D. ($n = 3$).

In fact, accumulation of $PrP^C$ in the cytoplasm is known to be strongly neurotoxic in both transgenic mice overexpressing the cytosolic form of $PrP^C$ [15] and cyclosporin A-treated cultured cells [7]. In these systems, $PrP^C$ expression enhances staurosporine-stimulated neuronal toxicity and DNA fragmentation, caspase-3-like activity and p53 transcriptional activities, all of which suggests that $PrP^C$ sensitizes neurons to apoptotic stimuli through caspase-3-mediated activation [20]. Proteasome inhibitors increase $PrP^C$-like immunoreactivity and unmask basal caspase-3 activation [19].

Despite these efforts, little is known about the $PrP^C$ localization and its metabolic fate in the cytoplasm. Ma et al. reported that PrP accumulated in the cytoplasm when proteasomal activity was compromised, and $PrP^C$ formed aggregates, often in association with Hsc70 [14]. With prolonged incubation, these aggregates accumulate in an "aggresome"-like state, surrounding the centrosome. Contrary to this report, other investigators reported there was a prominent shift in the intracellular locations of PrP immunostaining, but there was no "aggresome"-like PrP accumulation in the centrosome region [29]. The PrP signal was especially pronounced around the nucleus, and this signal only partially overlapped with both ER (calnexin, BiP and concanavalin A) and Golgi (wheat germ agglutinin). Thus, further examination has been awaited for determining the precise intracellular localization of $PrP^C$ in the cytoplasmic face.

With an artificial PrP peptide corresponding to PrP residues 106–126 [PrP(106–126)], chronic exposure of primary rat hippocampal cultures to micromolar concentrations of the peptide induces neuronal death with DNA fragmentation in degenerating neurons, having indicated apoptotic cell death [10]. The earliest detectable apoptotic event was the rapid depolarization of mitochondrial membranes, occurring immediately following treatment of cells with PrP(106–126). Subsequently, cytochrome *c* was released and caspase-3 was activated. It has also been demonstrated that the fusogenic peptide PrP(118–135) induced time- and dose-dependent apoptosis in rat cortical and retinal neurons that included caspase-3 activation and DNA condensation/fragmentation [4,22]. These results have implicated mitochondria as the primary site of action [18]. Unfortunately, this implication has been restricted to the cell death with the artificial PrP peptides, and thereby further illustrates the significance of our current observations in terms of the neurotoxic property of wild-type $PrP^C$ in vitro and in vivo.

There are potentially other mechanisms involved in neurotoxicity of the $PrP^{Sc}$-infected conditions, for example astrocytes, microglial cells and cytokines [17,25]. The activation of glial cells, which precedes neuronal death, and subsequent release of cytokines/chemokines may also contribute directly or indirectly to the neuronal cell death in prion diseases. In mutant $PrP^C$ metabolism, on the other hand, the ER also seems to play another important role as well. Mutant PrP(Q217R) remains associated with the chaperone BiP at the ER for an abnormally long period of time and is degraded by the proteasomal pathway [11]. Nonetheless, our current observations suggest that wild-type $PrP^C$ participate in the prion neurodegenerative cascade through the mitochondria-mediated events, at least in part. At the same time, the segregation of the infectious and neurotoxic properties of PrP suggests a new therapeutic strategy since prevention of mitochondrial mislocalization of $PrP^C$ can be regarded as putative therapeutic targets aimed at protecting

cells from mitochondria-mediated apoptosis, even though the prion infection is not fully preventable.

## Acknowledgements

We thank S.B. Prusiner for providing Tg(MoPrP)4053/FVB, T. Onodera for providing HpL3-4 cells, E. Nannri, K. Ishibashi, C. Ota, Y. Yamaura, and S. Wajima for technical assistance. We are indebted to G. Schatz, T. Omura, K. Mihara, R. Scheckman, and T. Momoi for helpful comments. This work was supported by grants from the Core Research for Evolutional Science and Technology (CREST) of the Japan Science and Technology Agency, Health and Labour Sciences Research Grants, Research on Advanced Medical Technology, nano-001, and the Ministry of Health, Labor and Welfare of Japan.

## References

[1] Y. Bounhar, Y. Zhang, C.G. Goodyer, A. LeBlanc, Prion protein protects human neurons against Bax-mediated apoptosis, J. Biol. Chem. 276 (2001) 39145–39149.
[2] S. Brandner, S. Isenmann, A. Raeber, M. Fischer, A. Sailer, Y. Kobayashi, S. Marino, C. Weissmann, A. Aguzzi, Normal host prion protein necessary for scrapie-induced neurotoxicity, Nature 379 (1996) 339–343.
[3] N. Canu, C. Barbato, M.T. Ciotti, A. Serafino, L. Dus, P. Calissano, Proteasome involvement and accumulation of ubiquitinated proteins in cerebellar granule neurons undergoing apoptosis, J. Neurosci. 20 (2000) 589–599.
[4] J. Chabry, C. Ratsimanohatra, I. Sponne, P.P. Elena, J.P. Vincent, T. Pillot, In vivo and in vitro neurotoxicity of the human prion protein (PrP) fragment P118–135 independently of PrP expression, J. Neurosci. 23 (2003) 462–469.
[5] L.B. Chiarini, A.R. Freitas, S.M. Zanata, R.R. Brentani, V.R. Martins, R. Linden, Cellular prion protein transduces neuroprotective signals, EMBO J. 21 (2002) 3317–3326.
[6] R. Chiesa, D.A. Harris, Prion diseases: what is the neurotoxic molecule? Neurobiol. Dis. 8 (2001) 743–763.
[7] E. Cohen, A. Taraboulos, Scrapie-like prion protein accumulates in aggresomes of cyclosporin A-treated cells, EMBO J. 22 (2003) 404–417.
[8] B. Drisaldi, R.S. Stewart, C. Adles, L.R. Stewart, E. Quaglio, E. Biasini, L. Fioriti, R. Chiesa, D.A. Harris, Mutant PrP is delayed in its exit from the endoplasmic reticulum, but neither wild-type nor mutant PrP undergoes retrotranslocation prior to proteasomal degradation, J. Biol. Chem. 278 (2003) 21732–21743.
[9] M.E. Figueiredo-Pereira, K.A. Berg, S. Wilk, A new inhibitor of the chymotrypsin-like activity of the multicatalytic proteinase complex (20S proteasome) induces accumulation of ubiquitin-protein conjugates in a neuronal cell, J. Neurochem. 63 (1994) 1578–1581.
[10] G. Forloni, N. Angeretti, R. Chiesa, E. Monzani, M. Salmona, O. Bugiani, F. Tagliavini, Neurotoxicity of a prion protein fragment, Nature 362 (1993) 543–546.
[11] T. Jin, Y. Gu, G. Zanusso, M. Sy, A. Kumar, M. Cohen, P. Gambetti, N. Singh, The chaperone protein BiP binds to a mutant prion protein and mediates its degradation by the proteasome, J. Biol. Chem. 275 (2000) 38699–38704.
[12] R.R. Kopito, ER quality control: the cytoplasmic connection, Cell 88 (1997) 427–430.
[13] C. Kuwahara, A.M. Takeuchi, T. Nishimura, K. Haraguchi, A. Kubosaki, Y. Matsumoto, K. Saeki, T. Yokoyama, S. Itohara, T. Onodera, Prions prevent neuronal cell-line death, Nature 400 (1999) 225–226.
[14] J. Ma, S. Lindquist, Wild-type and PrP and a mutant associated with prion disease are subject to retrograde transport and proteasome degradation, Proc. Natl. Acad. Sci. U.S.A. 98 (2001) 14955–14960.
[15] J. Ma, R. Wollmann, S. Lindquist, Neurotoxicity and neurodegeneration when PrP accumulates in the cytosol, Science 298 (2002) 1781–1785.
[16] G. Mallucci, A. Dickinson, J. Linehan, P.C. Klohn, S. Brandner, J. Collinge, Depleting neuronal PrP in prion infection prevents disease and reverses spongiosis, Science 302 (2003) 871–874.
[17] M. Marella, J. Chabry, Neurons and astrocytes respond to prion infection by inducing microglia recruitment, J. Neurosci. 24 (2004) 620–627.
[18] C.N. O'Donovan, D. Tobin, T.G. Cotter, Prion protein fragment PrP-(106–126) induces apoptosis via mitochondrial disruption in human neuronal SH-SY5Y cells, J. Biol. Chem. 276 (2001) 43516–43523.
[19] E. Paitel, C. Alves da Costa, D. Vilette, J. Grassi, F. Checler, Overexpression of PrPc triggers caspase 3 activation: potentiation by proteasome inhibitors and blockade by anti-PrP antibodies, J. Neurochem. 83 (2002) 1208–1214.
[20] E. Paitel, R. Fahraeus, F. Checler, Cellular prion protein sensitizes neurons to apoptotic stimuli through Mdm2-regulated and p53-dependent caspase 3-like activation, J. Biol. Chem. 278 (2003) 10061–10066.
[21] V. Perrier, K. Kaneko, J. Safar, J. Vergara, P. Tremblay, S.J. DeArmond, F.E. Cohen, S.B. Prusiner, A.C. Wallace, Dominant-negative inhibition of prion replication in transgenic mice, Proc. Natl. Acad. Sci. U.S.A. 99 (2002) 13079–13084.
[22] T. Pillot, B. Drouet, M. Pincon-Raymond, J. Vandekerckhove, M. Rosseneu, J. Chambaz, A nonfibrillar form of the fusogenic prion protein fragment [118-135] induces apoptotic cell death in rat cortical neurons, J. Neurochem. 75 (2000) 2298–2308.
[23] R.K. Plemper, D.H. Wolf, Retrograde protein translocation: ERADication of secretory proteins in health and disease, Trends Biochem. Sci. 24 (1999) 266–270.
[24] S.B. Prusiner, Prions, Proc. Natl. Acad. Sci. U.S.A. 95 (1998) 13363–13383.
[25] J. Schultz, A. Schwarz, S. Neidhold, M. Burwinkel, C. Riemer, D. Simon, M. Kopf, M. Otto, M. Baier, Role of interleukin-1 in prion disease-associated astrocyte activation, Am. J. Pathol. 165 (2004) 671–678.
[26] L. Solforosi, J.R. Criado, D.B. McGavern, S. Wirz, M. Sanchez-Alavez, S. Sugama, L.A. DeGiorgio, B.T. Volpe, E. Wiseman, G. Abalos, E. Masliah, D. Gilden, M.B. Oldstone, B. Conti, R.A. Williamson, Cross-linking cellular prion protein triggers neuronal apoptosis in vivo, Science 303 (2004) 1514–1516.
[27] G.C. Telling, T. Haga, M. Torchia, P. Tremblay, S.J. DeArmond, S.B. Prusiner, Interactions between wild-type and mutant prion proteins modulate neurodegeneration in transgenic mice, Genes Dev. 10 (1996) 1736–1750.
[28] D. Westaway, J. Cayetano-Canlas, D. Groth, D. Foster, S.-L. Yang, M. Torchia, G.A. Carlson, S.B. Prusiner, Degeneration of skeletal muscle, peripheral nerves, and the central nervous system in transgenic mice overexpressing wild-type prion proteins, Cell 76 (1994) 117–129.
[29] Y. Yedidia, L. Horonchik, S. Tzaban, A. Yanai, A. Taraboulos, Proteasomes and ubiquitin are involved in the turnover of the wild-type prion protein, EMBO J 20 (2001) 5383–5391.
[30] G. Zanusso, R.B. Petersen, T. Jin, Y. Jing, R. Kanoush, S. Ferrari, P. Gambetti, N. Singh, Proteasomal degradation and N-terminal protease resistance of the codon 145 mutant prion protein, J. Biol. Chem. 274 (1999) 23396–23404.
[31] H. Zhou, F. Cao, Z. Wang, Z.X. Yu, H.P. Nguyen, J. Evans, S.H. Li, X.J. Li, Huntingtin forms toxic $NH_2$-terminal fragment complexes that are promoted by the age-dependent decrease in proteasome activity, J. Cell Biol. 163 (2003) 109–118.

Available online at www.sciencedirect.com
SCIENCE DIRECT®
Biochemical and Biophysical Research Communications 327 (2005) 894–899
BBRC
www.elsevier.com/locate/ybbrc

# Prion protein with Y145STOP mutation induces mitochondria-mediated apoptosis and PrP-containing deposits in vitro

Naomi S. Hachiya[a,b], Kota Watanabe[a,b], Makiko Y. Kawabata[a,b], Akiko Jozuka[a,b], Yoshimichi Kozuka[c], Yuji Sakasegawa[a], Kiyotoshi Kaneko[a,b,*]

[a] *Department of Cortical Function Disorders, National Institute of Neuroscience (NIN), National Center of Neurology and Psychiatry (NCNP), Kodaira, Tokyo 187-8502, Japan*
[b] *Core Research for Evolutional Science and Technology (CREST), Japan Science and Technology Corporation, Japan*
[c] *Department of Ultrastructural Research, National Institute of Neuroscience (NIN), National Center of Neurology and Psychiatry (NCNP), Kodaira, Tokyo 187-8502, Japan*

Received 2 December 2004
Available online 29 December 2004

**Abstract**

A pathogenic truncation of an amber mutation at codon 145 (Y145STOP) in Gerstmann–Straussler–Scheinker disease (GSS) was investigated through the real-time imaging in living cells, by utilizing GFP-PrP constructs. GFP-PrP(1–144) exhibited an aberrant localization to mitochondria in mouse neuroblastoma neuro2a (N2a) and HpL3-4 cells, a hippocampal cell line established from *prnp* gene-ablated mice, whereas full-length GFP-PrP did not. The aberrant mitochondrial localization was also confirmed by Western blot analysis. Since GFP-PrP(1–121), as previously reported, and full-length GFP-PrP do not exhibit such mitochondrial localization, the mitochondrial localization of GFP-PrP(1–144) requires not only PrP residues 121–144 (in human sequence) but also COOH-terminal truncation in the current experimental condition. Subsequently, the GFP-PrP(1–144) induced a change in the mitochondrial innermembrane potential ($\Delta\Psi_m$), release of cytochrome *c* from the intermembrane space into the cytosol, and DNA fragmentation in these cells. Non-fluorescent PrP(1–144) also induced the DNA fragmentation in N2a and HpL3-4 cells after the proteasomal inhibition. These data may provide clues as to the molecular mechanism of the neurotoxic property of Y145STOP mutation. Furthermore, immunoelectron microscopy revealed numerous electron-dense deposits in mitochondria clusters of GFP-PrP(1–144)-transfected N2a cells, whereas no deposit was detected in the cells transfected with full-length GFP-PrP. Co-localization of GFP/PrP-immunogold particles with porin-immunogold particles as a mitochondrial marker was observed in such electron-dense vesicular foci, resembling those found in autophagic vacuoles forming secondary lysosomes. Whether such electron-dense deposits may serve as a seed for the growth of amyloid plaques, a characteristic feature of GSS with Y145STOP, awaits further investigations.


*Keywords:* Cellular prion protein; Green fluorescent protein; PrP Y145STOP mutation; Mitochondria-mediated apoptosis; PrP-containing deposits

Prion protein (PrP) consists of two isoforms, one is a host-encoded cellular isoform ($PrP^C$) and the other is an abnormal protease-resistant pathogenic isoform ($PrP^{Sc}$), of which the latter is a causative agent of prion disease. $PrP^{Sc}$ stimulates the conversion of $PrP^C$ into nascent $PrP^{Sc}$, and the accumulation of $PrP^{Sc}$ leads to central nervous system dysfunction and neuronal degeneration both in humans and animals [1]. The human prion diseases include kuru, Creutzfeldt–Jakob disease, Gerstmann–Straussler–Scheinker disease (GSS), and fatal familial insomnia [2,3].

* Corresponding author. Fax: +81 42 346 1748.
*E-mail address:* kaneko@ncnp.go.jp (K. Kaneko).

0006-291X/$ - see front matter © 2004 Elsevier Inc. All rights reserved.
doi:10.1016/j.bbrc.2004.12.079

We previously demonstrated the microtubule-associated intracellular localization of the $NH_2$-terminal fluorescent $PrP^C$ fragment [4] in mouse neuroblastoma neuro2a (N2a) and HpL3-4 cells, a hippocampal cell line established from *prnp* gene-ablated mice [5], by utilizing double-labeled $PrP^C$. We detected $NH_2$-terminally fluorescent-tagged $PrP^C$ predominantly in the intracellular compartments, COOH-terminally fluorescent-tagged $PrP^C$ mostly at the cell surface membranes overlapping with lipid rafts, and $PrP^C$ in full length with the merged color in Golgi compartments. Truncated $PrP^C$ with the amino acid residues 1–121, 1–111, and 1–91 in mouse PrP exhibited a proper distribution profile. Following real-time imaging analysis with GFP-$PrP^C$ revealed that the discrete $NH_2$-terminal amino acid residues are indispensable for the anterograde and the retrograde intracellular movements of GFP-$PrP^C$ [6]. Consistent with our reports, other groups also found the GFP-tagged version of $PrP^C$ to be properly anchored at the cell surface and its distribution pattern to be similar to that of the endogenous $PrP^C$, with labeling at the plasma membrane and in an intracellular perinuclear compartment [7–11].

Meanwhile, a pathogenic truncation of an amber mutation at codon 145 (Y145STOP) in the *prnp* gene, which was identified in a Japanese patient with GSS [12], came to our notice. The Y145STOP in human *prnp* gene corresponds to Y144STOP in mouse *prnp* gene which yields a product, mouse PrP(1–143) but hereafter designated PrP(1–144), and results in intracellular accumulation if proteasomal degradation is impaired [13]. Until now, its precise subcellular localization and relevance to the neurotoxic property have not been well characterized. Hence, GFP version of PrP(1–144) transgene was constructed and transfected in two independent cell lines, N2a and HpL3-4 cells.

Here we demonstrate for the first time that GFP-PrP(1–144) exhibited an aberrant mitochondrial localization accompanied by the depolarization of mitochondrial innermembrane, cytochrome *c* release in the cytosol, DNA fragmentation, and the formation of numerous PrP-containing deposits in intracellular vacuoles resembling secondary lysosomes.

## Materials and methods

*Construction of GFP-PrP and GFP-PrP(1–144).* GFP-PrP constructs were made as previously described [4,6], and the resulted plasmid was designated pSPOX-MHM2PrP::GFP. The mutant was amplified by PCR from the pSPOX-MHM2PrP::GFP (for amino acid residues Δ144–230 in mouse PrP) [4,6], digested with *Bam*HI and *Xho*I, and replaced with the *Bam*HI–*Xho*I fragment of pSPOX-MHM2PrP::GFP [14]. Non-fluorescent PrP constructs were made from the pSPOX-MHM2PrP [14]. The resulted plasmid was verified by direct DNA sequencing.

*Antibodies and drugs.* Antibody K3 against $PrP^C$ was rabbit polyclonal sera raised against N-terminal PrP peptides corresponding to residues 76–90 in mouse PrP. Anti-cytochrome *c* and anti-porin were purchased from BD Biosciences. Anti-Hsc70 and anti-BiP were purchased from Stressgen Biotechnologies. Anti-GFP was purchased from Sigma. Mitotracker Red CMXRos was purchased from Molecular Probes. Lactacystin, ALLN, and MG132 were purchased from Sigma. The mitochondrial innermembrane potential ($\Delta\Psi_m$) detection kit was purchased from Trevigen. DNA fragmentation was measured by TUNEL (APO-BrdU TUNEL assay kit (Molecular Probes)), which was performed according to the manufacturer's instructions before being visualized with a Delta-Vision microscopy system (Applied Precision), and out-of-focus images were removed by interactive deconvolution. Antibodies were used at 1:1000 (Western blotting) or 1:100 (immunoelectron microscopy) unless otherwise noted. For immunoelectron microscopy, 10 and 20 nm golds were purchased from DAKO.

*Cell cultures, DNA transfection, and drug treatments.* Mouse N2a cells were obtained from American Tissue Culture Collection, and HpL3-4 cells were provided by Dr. T. Onodera (the University of Tokyo). Cells were grown and maintained at 37 °C in MEM supplemented with 10% fetal bovine serum. N2a and HpL3-4 cells were transiently transfected with each construct using a DNA transfection kit (Lipofectamin, Gibco-BRL). Western blot analyses were performed as described [14]. To inhibit proteasomal function, N2a or HpL3-4 cells were treated with 10 μM lactacystin, ALLN, or MG132 for 3.5 h at 37 °C.

*Preparation of mitochondrial, microsomal, and cytosolic fractions [15].* Cells were homogenized with 9 volumes of mitochondrial buffer (220 mM mannitol, 70 mM sucrose, 10 mM Hepes–KOH, pH 7.4, and 0.1 mM EDTA) and centrifuged at 700*g* for 5 min at 4 °C, and the supernatant was further centrifuged at 5000*g* for 10 min at 4 °C. The supernatant was used as a post-mitochondrial supernatant. The resulted pellet was washed three times with mitochondrial buffer, resuspended in 9 volumes of the same buffer, and then centrifuged at 2000*g* for 2 min at 4 °C followed by 5000*g* for 8 min at 4 °C. The pellet was resuspended in 9 volumes of the same buffer and then centrifuged at 5000*g* for 10 min at 4 °C. The final pellet was recovered and stored on ice until use (mitochondrial fraction). The post-mitochondrial supernatant was further centrifuged at 100,000*g* for 1 h at 4 °C, and the supernatant was used as cytosolic fraction, and the pellet was resuspended in mitochondrial buffer (microsomal fraction). Western blots were performed at 5 μg total protein/lane.

*Real-time imaging.* To observe living cells, cells were cultured on glass-bottomed dishes (Matsunami) for 24–48 h after the DNA transfection. To visualize mitochondria, cells were incubated for 10 min at 37 °C with Mitotracker Red CMXRos at desired concentrations. Images of cells were collected with a Delta Vision Microscopy System (Applied Precision) equipped with an Olympus IX70.

## Results

The intracellular localization of fluorescent $PrP^C$ was investigated through the real-time imaging in living cells by utilizing GFP-PrP constructs. It was investigated in N2a cells that can be infected with $PrP^{Sc}$ [16] and has been widely used for studies in the $PrP^C$ metabolism, as well as in HpL3-4 cells, a hippocampal cell line established from *prnp* gene-ablated mice [5].

GFP-PrP(1–144) exhibited an aberrant localization to mitochondria, as demonstrated by its colocalization with the mitochondrial-specific molecule, Mitotracker, in N2a cells (Fig. 1A, upper panels) and HpL3-4 cells (Fig. 1A, lower panels), whereas full-length GFP-PrP did not. Previously, we also demonstrated that GFP-

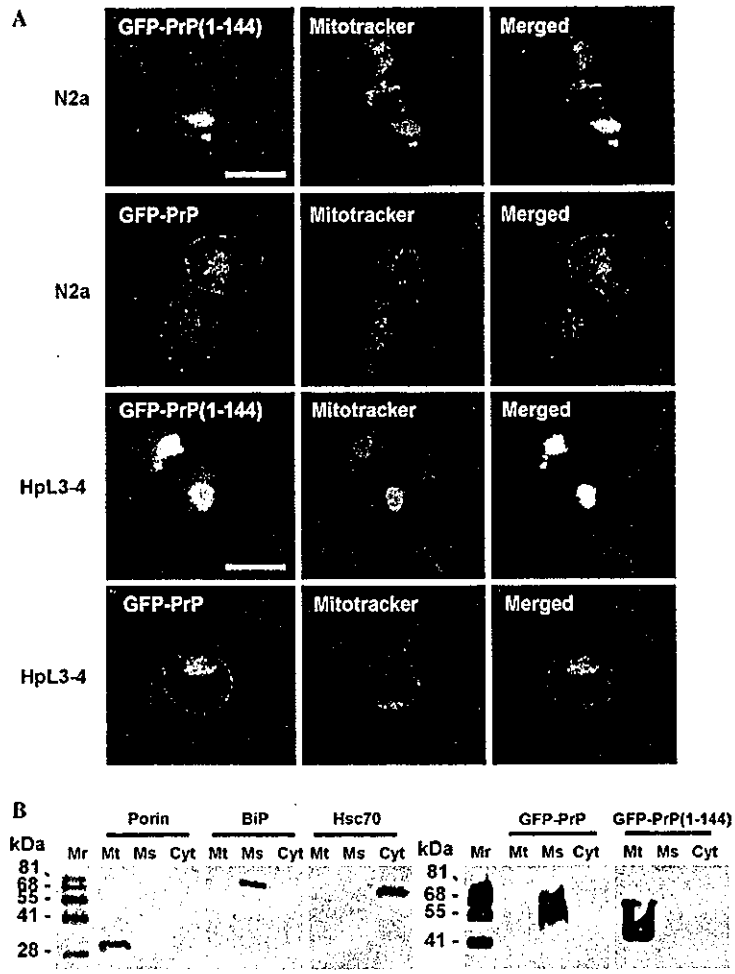


Fig. 1. Mitochondrial localization of GFP-PrP(1–144). GFP-PrP(1–144) exhibits aberrant localization in N2a cells, whereas full-length GFP-PrP does not. (A) GFP-PrP$^{C}$ localization. Full-length GFP-PrP and GFP-PrP(1–144) constructs were made and transfected in N2a (upper panels) and HpL3-4 cells (lower panels). Scale bars = 8 μm. (B) Western blot analysis with anti-GFP antibody. Anti-porin antibody was used as a mitochondrial (Mt) marker, anti-BiP antibody was used as a microsome (Ms) marker, and anti-Hsc70 antibody was used as a cytosolic (Cyt) marker. Mr, molecular weight marker.

PrP(1–121) does not exhibit such mitochondrial localization [4]. Thus, the mitochondrial localization of GFP-PrP(1–144) requires not only PrP residues 121–144 (in human sequence) but also COOH-terminal truncation in the current experimental condition, regardless of whether endogenous full-length PrP$^{C}$ exists. The aberrant mitochondrial localization of GFP-PrP(1–144) was further confirmed by Western blot analysis using a subcellular fractionation method (Fig. 1B).

Subsequently, the GFP-PrP(1–144) induced the depolarization of mitochondrial innermembrane (a change in the $\Delta\Psi_m$) in N2a (Fig. 2A, upper panels) and HpL3-4 cells (Fig. 2A, lower panels), release of cytochrome *c* from the intermembrane space into the cytosol (Fig. 2B), and DNA fragmentation assessed by TUNEL in N2a (Fig. 2C, upper panels) and HpL3-4 cells (data not shown). The PrP(1–144) is normally degraded through the proteasomal pathway, but intracellular accumulation results if proteasomal degradation is impaired [13]. Therefore, we next set out to treat the non-fluorescent PrP(1–144)-transfected cells with proteasome inhibitors including lactacystin, ALLN, or MG132. After the lactacystin treatment, non-fluorescent PrP(1–144) induced the DNA fragmentation in N2a (Fig. 2C, lower panels) and HpL3-4 cells (data not shown). Treatment with ALLN or MG132 also exhibited similar results (data not shown). These observations are characteristic of the mitochondria-mediated apoptotic process. In contrast, none of these abnormalities was observed in N2a and HpL3-4 cells transfected with full-length GFP-PrP construct.

During these investigations, we noticed that GFP-PrP(1–144)-transfected N2a and HpL3-4 cells lost its normal mitochondrial configurations as if congregated predominantly in an intracellular perinuclear region. To further investigate the ultrastructural

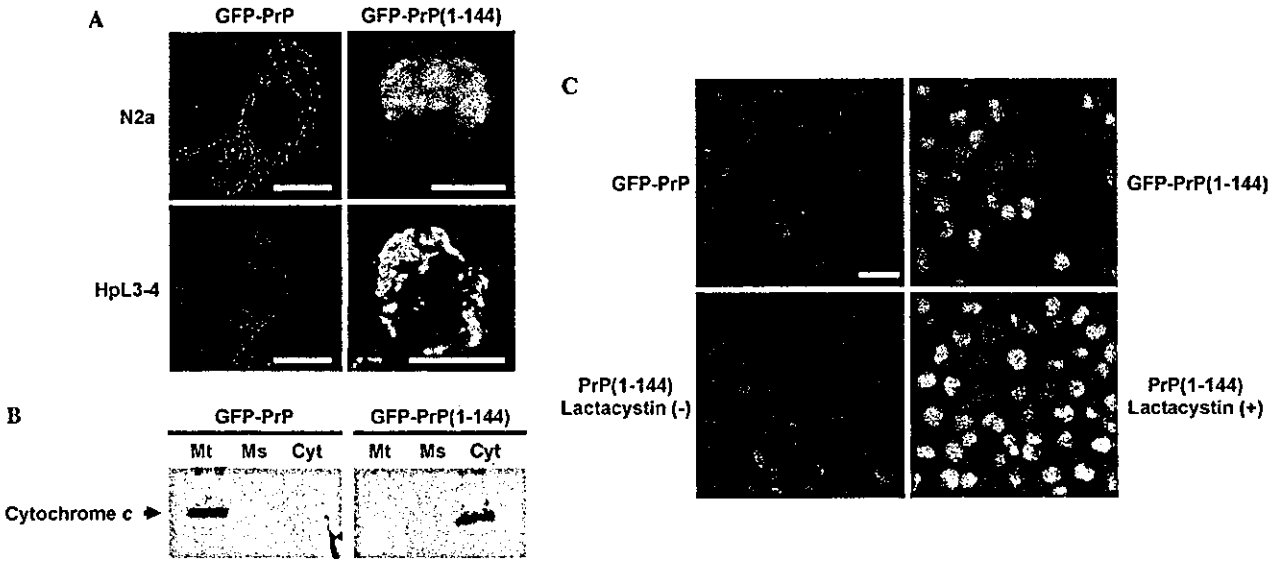


Fig. 2. Accumulation of GFP-PrP(1–144) induces mitochondria-mediated apoptosis. (A) Inactivation of the mitochondrial innermembrane potential ($\Delta\Psi_m$, red; active, green; inactive) in N2a (upper panels) and HpL3-4 (lower panels) cells transfected with GFP-PrP(1–144). Scale bars = 4 μm. (B) The release of cytochrome *c* from the mitochondria in N2a cells transfected with GFP-PrP(1–144). Mt, mitochondria fraction; Ms, microsome fraction; and Cyt, cytosolic fraction. The markers are the same as shown in Fig. 1B. (C) Upper panels: DNA fragmentations measured by TUNEL (red; negative, green; positive) are shown in N2a cells transfected with GFP-PrP(1–144). Lower panels: non-fluorescent PrP(1–144) transfected in N2a cells also exhibits the DNA fragmentation in a lactacystin-dependent manner. Scale bars = 15 μm.

morphology of these mitochondria, we next performed electron microscopy in N2a cells transfected with GFP-PrP(1–144) in comparison with full-length GFP-PrP.

As results, numerous electron-dense deposits were observed in mitochondrial clusters of the GFP-PrP(1–144)-transfected N2a cells, whereas none was detected in N2a cells transfected with full-length GFP-PrP (Fig. 3A). Some vesicles contained myelin-like figures resembling those found in autophagic vacuoles forming secondary lysosomes (Fig. 3B). Co-localization of PrP-immunogolds (Fig. 3C, left panel)/GFP-immunogolds (Fig. 3C, middle panel) with porin-immunogold particles as a mitochondrial marker (Fig. 3C, right panel) was observed in such electron-dense vesicular foci. Non-fluorescent PrP(1–144) also induced the same deposits after the proteasomal inhibition (data not shown).

## Discussion

The Y145STOP mutation at PrP residue 145 results in a heritable human prion disease, GSS-like disorder, with extensive PrP amyloid deposits in cerebral parenchyma and vessels [12,17]. The Y145STOP, which yields a product of PrP(1–144), lacks GPI-anchor and is normally degraded through the proteasomal pathway, and also results in intracellular accumulation if proteasomal degradation is impaired [13]. Most PrP(1–144) is degraded very rapidly by the proteasome-mediated pathway, and thus blockage of proteasomal degradation results in intracellular accumulation of PrP(1–144). From the current results, however, the GFP-tagged PrP(1–144) seems to be more metabolically stable, and therefore GFP-PrP(1–144) expression itself is sufficient to induce its intracellular accumulation. In fact, non-fluorescent PrP(1–144) required the treatment with proteasome inhibitors to exhibit the same features.

In this paper, we revealed for the first time the site of intracellular accumulation and the neurotoxic property of mutant $PrP^C$, Y145STOP, in a human GSS model. The GFP-PrP(1–144) exhibited an aberrant localization to mitochondria, and subsequent mitochondria-mediated apoptosis was induced. Misfolded $PrP^C$ is subjected to degradation by proteasomes, and accumulation of $PrP^C$ in the cytosol is strongly neurotoxic in transgenic mice [18] and cyclosporin A-treated cultured cells [19], and proteasome inhibitors increase $PrP^C$-like immunoreactivity and unmasked a basal caspase 3 activation [20]. Concomitant with decreased proteasomal activity, aberrant mitochondrial localization of $PrP^C$ followed by mitochondria-mediated neuronal apoptosis was also detected in aged transgenic mice overexpressing wild-type mouse $PrP^C$, but only after 520 days after birth [15]. These mice develop a spontaneous neurological dysfunction in an age-dependent manner [21,22]. Taken together, a $PrP^C$ load in the cytosol induces the mitochondrial localization of $PrP^C$ with subsequent mito-

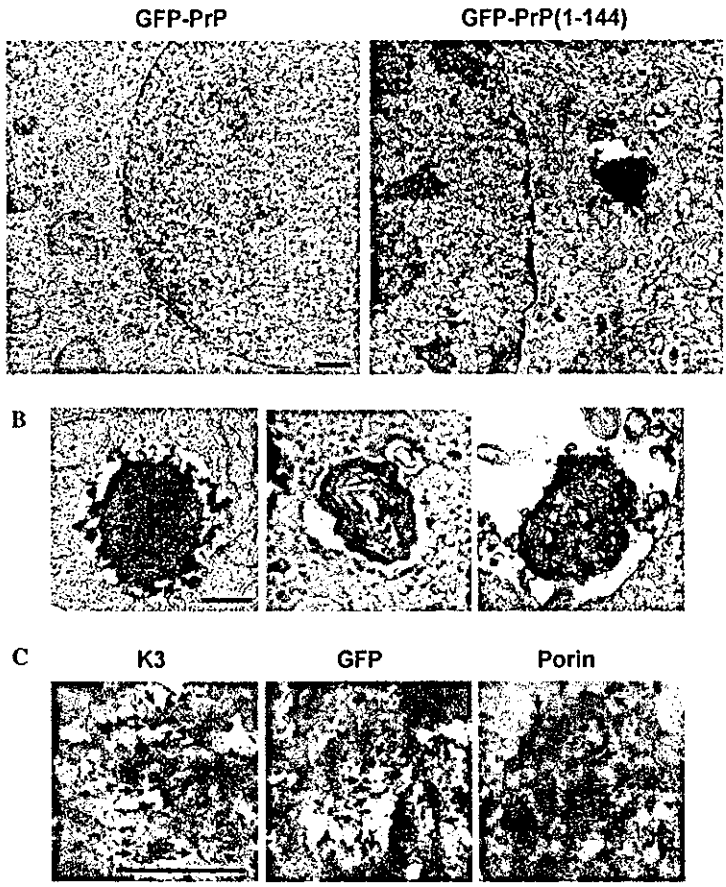


Fig. 3. GFP-PrP(1–144)-related electron-dense deposits. Scale bars = 0.1 μm. (A) Electron microscopy (30,000×) detects numerous electron-dense deposits in N2a cells transfected with GFP-PrP(1–144), whereas full-length GFP-PrP induces no deposit. (B) Some vesicles contain myelin-like figures. (C) Immunoelectron microscopy (30,000×) detects GFP-PrP(1–144) with anti-PrP antibody K3 (10 nm golds, left panel) or anti-GFP antibody (10 nm golds, middle panel) within the electron dense deposits of N2a cells. Anti-porin antibody (20 nm golds) also stains the deposits (right panel).

chondria-mediated apoptosis. Consequently, such neurotoxic property may contribute to a common pathogenic mechanism shared in various PrP-related disorders.

Deposition of numerous electron-dense deposits immunostained with anti-PrP antibody is another characteristic in GFP-PrP(1–144)-transfected cells, and has not been reported in other studies so far. The relevance of such electron-dense deposits with PrP amyloid deposits, a characteristic feature of human GSS with Y145STOP, is an intriguing question. These amyloid plaques were composed of COOH-terminal truncated PrP [12], but have not transmitted to mice [17]. Of note, both the electron-dense deposits in Y145STOP-transfected N2a cells and $PrP^{Sc}$ in scrapie-infected N2a cells were found in the similar vacuolar compartment resembling secondary lysosomes [23], suggesting that both deposits may share a similar resistance to such a harsh lysosomal condition.

The Y145STOP mutation has been widely investigated in terms of its biochemical property. Peptides encompassing PrP(89–143) when mixed with $PrP^{C}$ produced fibrous aggregates and displayed a high β-sheet content, although no prion infectivity was observed [24,25]. Recently, Kundu et al. [26] reported a spontaneous conversion of the recombinant polypeptide, human PrP(23–144), from a monomeric unordered state to a fibrillar form, in which human PrP residues within the 138–141 region are essential. Interestingly, this conversion has characteristics of a nucleation-dependent polymerization. Whether the numerous electron-dense deposits may serve as a seed for the growth of amyloid plaques with Y145STOP awaits further investigations.

Our current observations may provide clues as to the yet unknown underlying mechanism concerning the heritable human prion disease with Y145STOP at least in part. At the same time, the prion disease with Y145STOP has untransmitted to mice [17]. How this relates to the puzzle in prion biology, the discrepancy between the infectious and neurotoxic properties of PrP [27], remains to be further examined.

## Acknowledgments

We greatly thank T. Onodera for providing the HpL3-4 cell line, E. Nannri, K. Ishibashi, C. Ota, and S. Wajima for technical assistances. This work was supported by grants from the Core Research for Evolutional Science and Technology (CREST) of Japan Science and Technology Corporation, Health and Labour Sciences Research Grants, Research on Advanced Medical Technology, nano-001, the Ministry of Agriculture, Forestry and Fisheries, and the Ministry of Health, Labor, and Welfare of Japan.

## References

[1] S.B. Prusiner, Prions, Proc. Natl. Acad. Sci. USA 95 (1998) 13363–13383.
[2] S.B. Prusiner, Shattuck lecture—neurodegenerative diseases and prions, N. Engl. J. Med. 344 (2001) 1516–1526.
[3] J. Collinge, Variant creutzfeldt-Jakob disease, Lancet 354 (1999) 317–323.
[4] N.S. Hachiya, K. Watanabe, Y. Sakasegawa, K. Kaneko, Microtubules-associated intracellular localization of the NH(2)-terminal cellular prion protein fragment, Biochem. Biophys. Res. Commun. 313 (2004) 818–823.
[5] C. Kuwahara, A.M. Takeuchi, T. Nishimura, K. Haraguchi, A. Kubosaki, Y. Matsumoto, K. Saeki, T. Yokoyama, S. Itohara, T. Onodera, Prions prevent neuronal cell-line death, Nature 400 (1999) 225–226.
[6] N.S. Hachiya, K. Watanabe, M. Yamada, Y. Sakasegawa, K. Kaneko, Anterograde and retrograde intracellular trafficking of fluorescent cellular prion protein, Biochem. Biophys. Res. Commun. 315 (2004) 802–807.
[7] K.S. Lee, A.C. Magalhaes, S.M. Zanata, R.R. Brentani, V.R. Martins, M.A. Prado, Internalization of mammalian fluorescent cellular prion protein and N-terminal deletion mutants in living cells, J. Neurochem. 79 (2001) 79–87.
[8] A.C. Magalhaes, J.A. Silva, K.S. Lee, V.R. Martins, V.F. Prado, S.S.G. Ferguson, M.V. Gomez, R.R. Brentani, M.A.M. Prado, Endocytic intermediates involved with the intracellular trafficking of a fluorescent cellular prion protein, J. Biol. Chem. 277 (2002) 33311–33318.
[9] A. Negro, C. Ballarin, A. Bertoli, M.L. Massimino, M.C. Sorgato, The metabolism and imaging in live cells of the bovine prion protein in its native form or carrying single amino acid substitutions, Mol. Cell. Neurosci. 17 (2001) 521–538.
[10] H. Lorenz, O. Windl, H.A. Kretzschmar, Cellular phenotyping of secretory and nuclear prion proteins associated with inherited prion diseases, J. Biol. Chem. 277 (2002) 8508–8516.
[11] L. Ivanova, S. Barmada, T. Kummer, D.A. Harris, Mutant prion proteins are partially retained in the endoplasmic reticulum, J. Biol. Chem. 276 (2001) 42409–42421.
[12] T. Kitamoto, R. Iizuka, J. Tateishi, An amber mutation of prion protein in Gerstmann-Straussler syndrome with mutant PrP plaques, Biochem. Biophys. Res. Commun. 192 (1993) 525–531.
[13] G. Zanusso, R.B. Petersen, T. Jin, Y. Jing, R. Kanoush, S. Ferrari, P. Gambetti, N. Singh, Proteasomal degradation and N-terminal protease resistance of the codon 145 mutant prion protein, J. Biol. Chem. 274 (1999) 23396–23404.
[14] M.R. Scott, R. Kohler, D. Foster, S.B. Prusiner, Chimeric prion protein expression in cultured cells and transgenic mice, Protein Sci. 1 (1992) 986–997.
[15] N.S. Hachiya, M. Yamada, K. Watanabe, A. Jozuka, T. Ohkubo, K. Sano, Y. Takeuchi, Y. Kozuka, Y. Sakasegawa, K. Kaneko, Mitochondrial localization of cellular prion protein (PrPC) invokes neuronal apoptosis in aged transgenic mice overexpressing PrPC, Neurosci. Lett., in press.
[16] D.A. Butler, M.A. Scott, J.M. Bockman, D.R. Borchelt, A. Taraboulos, K.K. Hsiao, D.T. Kingsbury, S.B. Prusiner, Scrapie-infected murine neuroblastoma cells produce protease-resistant prion proteins, J. Virol. 62 (1988) 1558–1564.
[17] J. Tateishi, T. Kitamoto, Inherited prion diseases and transmission to rodents, Brain Pathol. 5 (1995) 53–59.
[18] J. Ma, R. Wollmann, S. Lindquist, Neurotoxicity and neurodegeneration when PrP accumulates in the cytosol, Science 298 (2002) 1781–1785.
[19] E. Cohen, A. Taraboulos, Scrapie-like prion protein accumulates in aggresomes of cyclosporin A-treated cells, EMBO J. 22 (2003) 404–417.
[20] E. Paitel, C. Alves da Costa, D. Vilette, J. Grassi, F. Checler, Overexpression of PrPc triggers caspase 3 activation: potentiation by proteasome inhibitors and blockade by anti-PrP antibodies, J. Neurochem. 83 (2002) 1208–1214.
[21] D. Westaway, J. Cayetano-Canlas, D. Groth, D. Foster, S.-L. Yang, M. Torchia, G.A. Carlson, S.B. Prusiner, Degeneration of skeletal muscle, peripheral nerves, and the central nervous system in transgenic mice overexpressing wild-type prion proteins, Cell 76 (1994) 117–129.
[22] V. Perrier, K. Kaneko, J. Safar, J. Vergara, P. Tremblay, S.J. DeArmond, F.E. Cohen, S.B. Prusiner, A.C. Wallace, Dominant-negative inhibition of prion replication in transgenic mice, Proc. Natl. Acad. Sci. USA 99 (2002) 13079–13084.
[23] M.P. McKinley, A. Taraboulos, L. Kenaga, D. Serban, A. Stieber, S.J. DeArmond, S.B. Prusiner, N. Gonatas, Ultrastructural localization of scrapie prion proteins in cytoplasmic vesicles of infected cultured cells, Lab. Invest. 65 (1991) 622–630.
[24] K. Kaneko, D. Peretz, K.M. Pan, T.C. Blochberger, H. Wille, R. Gabizon, O.H. Griffith, F.E. Cohen, M.A. Baldwin, S.B. Prusiner, Prion protein (PrP) synthetic peptides induce cellular PrP to acquire properties of the scrapie isoform, Proc. Natl. Acad. Sci. USA 92 (1995) 11160–11164.
[25] K. Kaneko, H. Wille, I. Mehlhorn, H. Zhang, H. Ball, F.E. Cohen, M.A. Baldwin, S.B. Prusiner, Molecular properties of complexes formed between the prion protein and synthetic peptides, J. Mol. Biol. 270 (1997) 574–586.
[26] B. Kundu, N.R. Maiti, E.M. Jones, K.A. Surewicz, D.L. Vanik, W.K. Surewicz, Nucleation-dependent conformational conversion of the Y145Stop variant of human prion protein: structural clues for prion propagation, Proc. Natl. Acad. Sci. USA 100 (2003) 12069–12074.
[27] R. Chiesa, P. Piccardo, E. Quaglio, B. Drisaldi, S.L. Si-Hoe, M. Takao, B. Ghetti, D.A. Harris, Molecular distinction between pathogenic and infectious properties of the prion protein, J. Virol. 77 (2003) 7611–7622.

Available online at www.sciencedirect.com
SCIENCE DIRECT®
Biochemical and Biophysical Research Communications 313 (2004) 818–823
BBRC
www.elsevier.com/locate/ybbrc

# Microtubules-associated intracellular localization of the $NH_2$-terminal cellular prion protein fragment

Naomi S. Hachiya, Kota Watanabe, Yuji Sakasegawa, and Kiyotoshi Kaneko*

*Department of Cortical Function Disorders, National Institute of Neuroscience (NIN), National Center of Neurology and Psychiatry (NCNP), Tokyo 187-8502, Japan*
*Core Research for Evolutional Science and Technology (CREST), Japan Science and Technology Corporation, Japan*

Received 25 November 2003

**Abstract**

By utilizing double-labeled fluorescent cellular prion protein ($PrP^C$), we revealed that the $NH_2$-terminal and COOH-terminal $PrP^C$ fragments exhibit distinct distribution patterns in mouse neuroblastoma neuro2a (N2a) cells and HpL3-4, a hippocampal cell line established from *prnp* gene-ablated mice [Nature 400 (1999) 225]. Of note, the $NH_2$-terminal $PrP^C$ fragment, which predominantly localized in the intracellular compartments, congregated in the cytosol after the treatment with a microtubule depolymerizer (nocodazole). Truncated $PrP^C$ with the amino acid residues 1–121, 1–111, and 1–91 in mouse (Mo) PrP exhibited a proper distribution profile, whereas those with amino acid residues 1–52 and 1–33 did not. These data indicate the microtubules-associated intracellular localization of the $NH_2$-terminal $PrP^C$ fragment containing at least the 1–91 amino acid residues.


*Keywords:* Prion protein; Microtubules; Fluorescent protein; Nocodazole; Proteolytic cleavage; Subcellular localization

Prion diseases are a group of neurodegenerative disorders including kuru, Creutzfeldt–Jakob disease (CJD), Gerstmann–Sträussler–Scheinker disease (GSS), and fatal familial insomnia (FFI) in humans, scrapie in sheep, and bovine spongiform encephalopathy (BSE) in cattle, which can be presented as sporadic, inherited, and infectious disorders [2]. The posttranslational conformational change of the cellular isoform of prion protein ($PrP^C$) into the scrapie isoform of prion protein ($PrP^{Sc}$) is the fundamental process underlying the pathogenesis of the prion disease [3,4]. After $PrP^C$ is synthesized in the endoplasmic reticulum, it transits through the Golgi apparatus to the cell surface lipid rafts which is a subcellular compartment defined biochemically by membranes rich in cholesterol and glycosphingolipids, where it is bound by a glycophosphatidylinositol (GPI)-anchor [5,6] and then $PrP^C$ is either metabolized or converted into $PrP^{Sc}$ [7–9].

Several groups have already generated fluorescent $PrP^C$ molecules, in which a green fluorescent protein (GFP) was either $NH_2$-terminally or COOH-terminally fused [10–13]. Of note, the copper treatment induced fluorescent $PrP^C$ to be internalized like endogenous $PrP^C$, indicating that such fluorescent $PrP^C$ could be functional [10]. Regardless of the position of the GFP inserts, fluorescent $PrP^C$ in a GPI-anchored form was reported as being correctly targeted to the plasma membrane, where it is detected in lipid rafts [10,12]. However, there has been neither direct comparison of distribution profiles between $NH_2$-terminally and COOH-terminally fluorescent-tagged $PrP^C$.

With this background, we made fluorescent PrP constructs double-labeled at both $NH_2$- and COOH-termini, and then investigated the subcellular localization in mouse neuroblastoma neuro2a (N2a) cells, known to be infectable with $PrP^{Sc}$ [14], and HpL3-4, a hippocampal cell line established from *prnp* gene-ablated mice [1]. Subsequently, we are tempted to investigate the association of the $NH_2$-terminal $PrP^C$ fragment with cytoskeletal proteins such as microtubules and actin.

* Corresponding author. Fax: +81-42-346-1748.
*E-mail address:* kaneko@ncnp.go.jp (K. Kaneko).

0006-291X/$ - see front matter © 2003 Elsevier Inc. All rights reserved.
doi:10.1016/j.bbrc.2003.11.167

## Materials and methods

*Construction of fluorescent PrP and the deletion mutants.* To express fluorescent PrP in mouse neuroblastoma cells, the EGFP gene was amplified by PCR from pEGFP (Clontech) using primers 5′-GACC GGTATGGTGAGCAAGGGCGAGGAGCTG-3′ and 5′-GACCG GTATGGTGAGCAAGGGCGAGGAGCTG-3′, digested with *Age*I, and inserted into the *Age*I site (between amino acid residues 34 and 35 in mouse (Mo) PrP) of pSPOX-MHM2PrP (a gift from Dr. S.B. Prusiner, University of California, San Francisco) [15] and the resulted plasmid was designated pSPOX-MHM2PrP::GFP. The series of deletion mutants were amplified by PCR from the pSPOX-MHM2PrP::GFP using 5′-CGGGATCCACCATGGCGAACCTTG GCTACTGGCTG-3′ as the forward primer and the following backward primers: 5′-CCG CTCGAGTCACTTGTACAGCTCGTCCATGCCGAGA-3′ (for amino acid residues 1–33 in Mo PrP), 5′-CCGCTCGAGTCACTGA GGTGGGTAACGGTT-3′ (1–52), 5′-CCGCTCGAGTCATCCTTG GCCCCATCCACC-3′ (1–91), 5′-CCGCTCGAGTCACATATGCTT CATGTTGGT-3′ (1–111), and 5′-CCGCTCGAGTCACACTACTG CCCCAGCTGC-3′ (1–121), digested with *Bam*HI and *Xho*I, and replaced with the *Bam*HI–*Xho*I fragment of pSPOX-MHM2PrP::GFP. The resulted plasmids were verified by direct DNA sequencing.

*Antibodies, organelle markers, and drugs.* Anti-PrP antibodies K1, K3, and K9 were rabbit polyclonal serum raised against the $NH_2$-termianl PrP peptides (amino acid residues 26–40, 76–90, and 196–210 in Mo PrP, respectively). Anti-COOH-terminal polyclonal $PrP^C$ antibody M20 and anti-tubulin antibody DM1A were purchased from Santa Cruz Biotechnology and Sigma, respectively. A Golgi marker anti-GM130 and a marker for lipid raft anti-GM1 antibody were purchased from BD Biosciences and Calbiochem, respectively. As ER markers, ER-Tracker Blue-White DPX (Molecular Probes), Calnexin (Stressgen), BiP (BD Biosciences), and PDI (Stressgen) were purchased and used. Other organelle markers including an early endosomal marker EEA1 (BD Biosciences), a lysosomal marker LysoTracker Green (Molecular Probes), and a mitochondrial marker MitoTracker Red CHXROS (Molecular Probes) were also used for the experiments. Nocodazole was purchased from Sigma.

*Cell cultures, DNA transfection, and drug treatments.* Mouse neuroblastoma neuro2a (N2a) cells were obtained from American Tissue Culture Collection. A hippocampal cell line established from *prnp* gene-ablated mice (HpL3-4) was kindly provided by Dr. T. Onodera. Cells were grown and maintained at 37 °C in MEM supplemented with 10% fetal bovine serum. N2a and HpL3-4 cells were transiently transfected with each construct using a DNA transfection kit (Lipofectamin, Gibco-BRL). Western blot analyses were performed as described [15]. Nocodazole treatment (30 μM at 30 °C for 0, 30, and 180 min) was performed according to the previous report [16].

*Immunofluorescent and fluorescence microscopy.* For indirect immunofluorescence analysis, fluorescent $PrP^C$-transfected cells were rinsed with PBS with $Ca^{2+}$ and $Mg^{2+}$ (PBS(+)) and then fixed with 10% formalin in 70% PBS(+) at room temperature for 30 min. After four washes with PBS(−), the fixed cells were incubated with 10% FBS in PBS(−) at room temperature for 30 min. They were then incubated at room temperature for 1 h with antibodies at desired concentrations. After four washes with PBS(−), the cells were incubated with either Alexa488 (green) Fluor-conjugated anti-rabbit IgG (Molecular Probes) or Alexa594 (red) Fluor-conjugated anti-mouse IgG (Molecular Probes), diluted 1:200 in PBS, at room temperature for 1 h. The stained cells were washed four times with PBS(−) and mounted with SLOW FADE (Molecular Probes). Immunofluorescent or autofluorescent samples were imaged with Delta-Vision microscopy system (Applied Precision), out of focus light of the visualized images was removed by interactive deconvolution.

*Immunoprecipitation of tubulin and $PrP^C$ from the tubulin–$PrP^C$ containing vesicular complex.* Harvested N2a cells (13 dishes of 9 cm plate) were washed with PBS(−) twice, suspended in PEM buffer (100 mM Pipes, 2 mM EDTA, and 1 mM $MgCl_2$) containing protease inhibitors (5 μM each of leupeptin, pepstatin, aprotinin, antipain, and 1 mM PMSF), and homogenized 30 times at 4 °C. The homogenates were centrifuged at 3000*g* for 3 min followed by 100,000*g* at 4 °C for 30 min and then the supernatant was recovered. To stabilize tubulin, the supernatant was treated with taxol (20 μM) with 1 mM GTP at 37 °C for 20 min and kept on ice for 10 min. Monoclonal anti-tubulin antibody DM1A was adsorbed to protein A–cellurofine in PBS at 4 °C for 5 h and then used for the immunoprecipitation. $PrP^C$ signals were detected by Western blotting with either K1 or K9 from the immunoprecipitated complex. Polyclonal K1 and K9 are suitable for Western blotting (data not shown).

## Results

### *Subcellular localization of fluorescent $PrP^C$*

The subcellular localization of fluorescent $PrP^C$ was investigated by utilizing double-labeled $PrP^C$, GFP–PrP–DsRed, and vice versa in N2a cells (Fig. 1A). We detected a $NH_2$-terminal $PrP^C$ fragment predominantly in intracellular compartments as a dot-like distribution pattern, a COOH-terminal $PrP^C$ fragment mostly at the cell surface, and $PrP^C$ in full length intracellularly (Fig. 1B). These results were in accordance with the behavior of endogenous $PrP^C$ immunostained with anti-PrP polyclonal antibodies K3 against the $NH_2$-terminal residues 76–90 in Mo PrP (Fig. 1C, left panel), and M20 against the COOH-terminal residues in Mo PrP (Fig. 1C, right panel) and thus, excluding the possibility of an artificial distribution of fluorescent $PrP^C$ by fusing the fluorescent proteins.

While a large proportion of intracellular $PrP^C$ was co-localized with a Golgi marker (anti-GM130) (data not shown), signals on plasma membranes were co-localized with a marker for lipid rafts (anti-GM1) (data not shown). These results are consistent with the previous observations [11–13,17]. However, under our culture conditions with N2a and HpL3-4 cells, we were unable to demonstrate co-localization of the intracellular $NH_2$-terminal $PrP^C$ fragment in a dot-like distribution pattern with known organelle markers such as ER (ER-Tracker Blue-White DPX, Calnexin, BiP, PDI), Golgi apparatus (GM130), early endosomes (EEA1), lysosomes (LysoTracker, Green), or mitochondria (MitoTracker Red CHXROS) (data not shown). Thus, such intracellular $PrP^C$ may not reflect the distribution to any single specific organelle, but further examination has yet to be required.

Western blot analysis with polyclonal antibody K1 against the $NH_2$-terminal residues 26–40 in Mo PrP detected the $NH_2$-terminal $PrP^C$ fragment of 17 kDa exclusively in a non-lipid raft fraction (data not shown). Further mapping of the $NH_2$-terminal $PrP^C$ cleavage site was achieved by transiently expressing 3F4 (amino acids 108/111 in Mo PrP) [18] epitope-tagged MHM2 $PrP^C$ in N2a cells. Again, 3F4 detected the $NH_2$-terminal $PrP^C$ fragment in the non-lipid raft fraction (Fig. 1D). Taken together, these data indicate that such $NH_2$-terminal

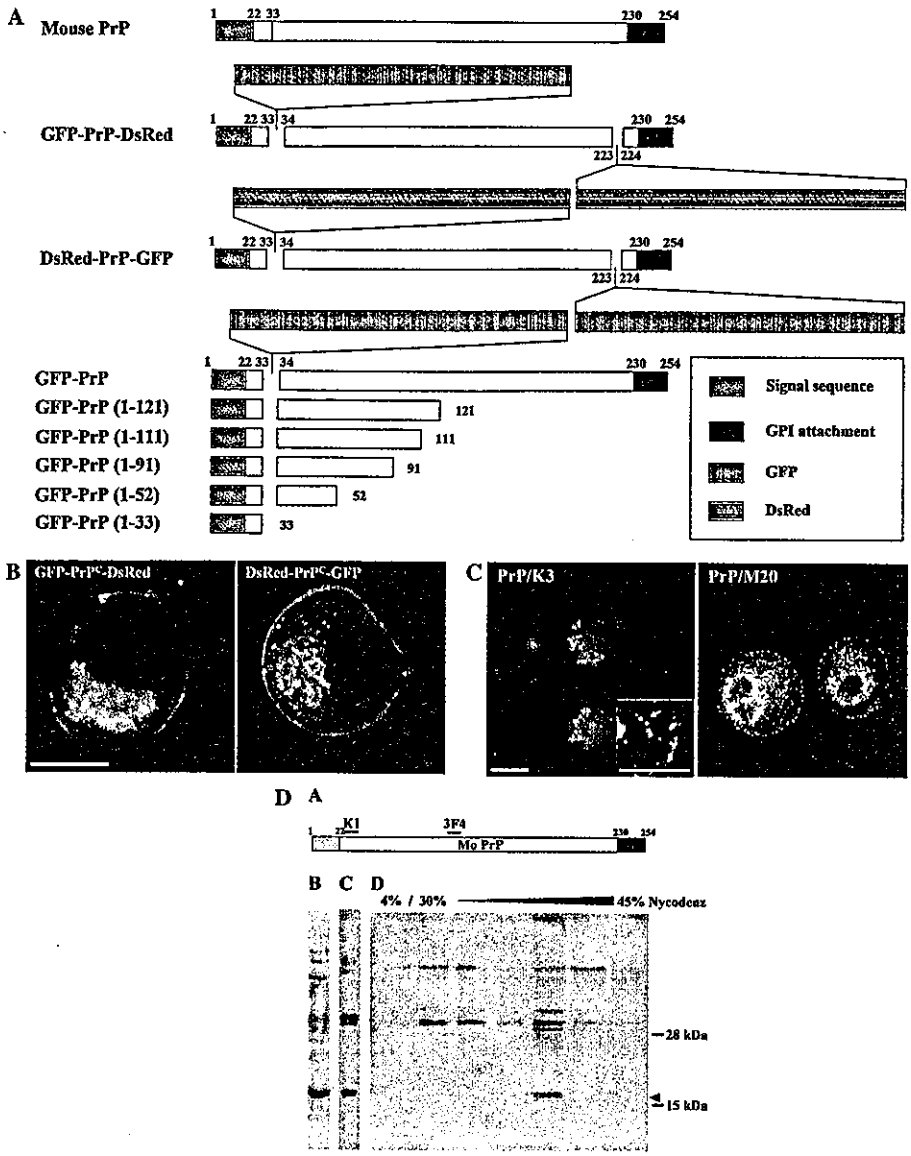


Fig. 1. Immunofluorescent analysis of fluorescent $PrP^C$. (A) The chimeric fluorescent PrP constructs (GFP–PrP–DsRed, DsRed–PrP–GFP, and the deletion mutant series,) used in this study. (B) Distribution patterns of GFP–PrP–DsRed (left panel): GFP–$PrP^C$ (green) predominantly in the intracellular vesicles, $PrP^C$–DsRed (red) mostly at the cell surface membranes, and GFP–$PrP^C$–DsRed (yellow) in intracellular compartments. The DsRed–PrP–GFP (right panel) exhibits an inverted color profile indicating the same distribution patterns independent of the fluorescent conjugates. Scale bar = 8 μm. (C) Endogenous $PrP^C$ is immunostained with anti-PrP polyclonal antibody K3 at a dilution of 1:200 (left panel) or M20 at a dilution of 1:200 (right panel). N2a cells were permeabilized with 0.1% Triton X-100. A distinct proportion of $PrP^C$ is detected in a dot-like distribution pattern (an arrow). Scale bars = 15 μm. (D) 3F4 detects $NH_2$-terminal MHM2 $PrP^C$ fragment of 17 kDa (arrow head) which was transiently transfected in N2a cells. To separate non-lipid raft fractions which contain high density, Triton X-100-insoluble intracellular membranes, we used the procedure of Naslavsky et al. [33] with slight modifications as below. Cells were lysed and resuspended in ice-cold buffer A (25 mM Hepes–KOH, pH 7.5, 5 mM EDTA, and 0.15 M NaCl) containing 1% Triton X-100, and then adjusted to 50% Nycodenz containing buffer A. Samples were centrifuged at 200,000*g* at 4 °C for 4 h by floatation in 1.5 ml of a discontinuous Nycodenz gradient (4/30/32.5/35/37.5/40/42.5/45%). After the centrifugation, samples were fractionated by 0.2 ml from the top of gradients.

$PrP^C$ fragment contains at least residues 26–40, 76–90, and 108/111 in Mo PrP.

*Microtubules-dependent intracellular localization of fluorescent $PrP^C$*

These observations of the intracellular $NH_2$-terminal $PrP^C$ fragment in a dot-like distribution pattern prompted us to further investigate its possible association with cytoskeletal proteins such as microtubules or actin. Co-immunostaining of endogenous $PrP^C$ and microtubules by anti-PrP polyclonal antibody K3/anti-tubulin monoclonal antibody DM1A detected $PrP^C$ along microtubules in N2a cells (Fig. 2) as well as HpL3-4 cells (data not shown). Subsequently, an immunoprecipitation assay performed with anti-tubulin antibody

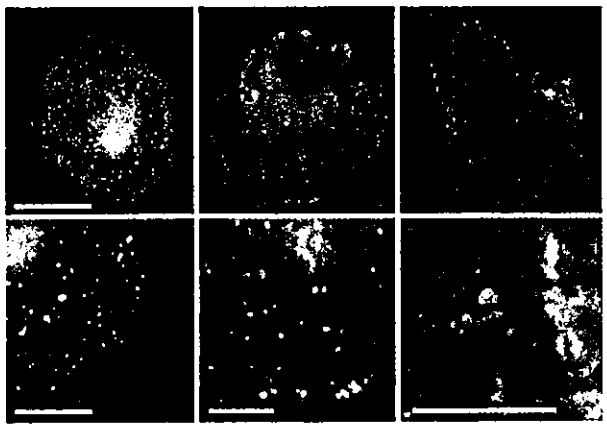

Fig. 2. Co-immunostaining of endogenous $PrP^C$ and microtubules by anti-PrP antibody K3 (1:200, green) and anti-tubulin antibody DM1A (1:200, red) detects $PrP^C$ along microtubules in N2a cells. Scale bar (upper panels) = 7 μm and scale bars (lower panels) = 3 μm.

(DM1A) resulted in the co-immunoprecipitation of tubulin and the $NH_2$-terminal $PrP^C$ fragment of 17 kDa in N2a cells (Fig. 3A). Another polyclonal antibody K9 against the COOH-terminal residues 196–210 in Mo PrP failed to detect COOH-terminal $PrP^C$ in the immunoprecipitated complex (Fig. 3A).

After N2a cells (Fig. 3B) were treated with 30 μM nocodazole which depolymerizes microtubules, the signals of GFP–$PrP^C$ were congregated in a time-dependent manner. On the other hand, latrunculin A, which is widely used as an agent to sequester monomeric actin in living cells, did not affect the localization of GFP–$PrP^C$ (data not shown). Finally, the deletion mutants (Fig. 1A) were used to map the amino acid residues responsible for the microtubules-associated localization of GFP–$PrP^C$. As shown in Fig. 3C, truncated constructs with the amino acid residues 1–121, 1–111, and 1–91 in Mo PrP exhibited its proper localization, whereas those with amino acid residues 1–52 and 1–33 in Mo PrP lost the dot-like distribution pattern.

## Discussion

First of all, our double-labeled fluorescent $PrP^C$ detected the $NH_2$-terminal and COOH-terminal $PrP^C$ fragments with distinct subcellular distribution profiles, in which cleavage of $PrP^C$ at around a middle region was involved [7,19,20].

Initial studies performed on the internalization of $PrP^C$ using a chicken $PrP^C$ have determined that endocytosis of chicken PrP is mediated by clathrin-coated pits, and the $NH_2$-terminal half of the chicken PrP polypeptide is essential for its endocytosis [21,22]. Recently, Nunziante et al. [23] also reported that the

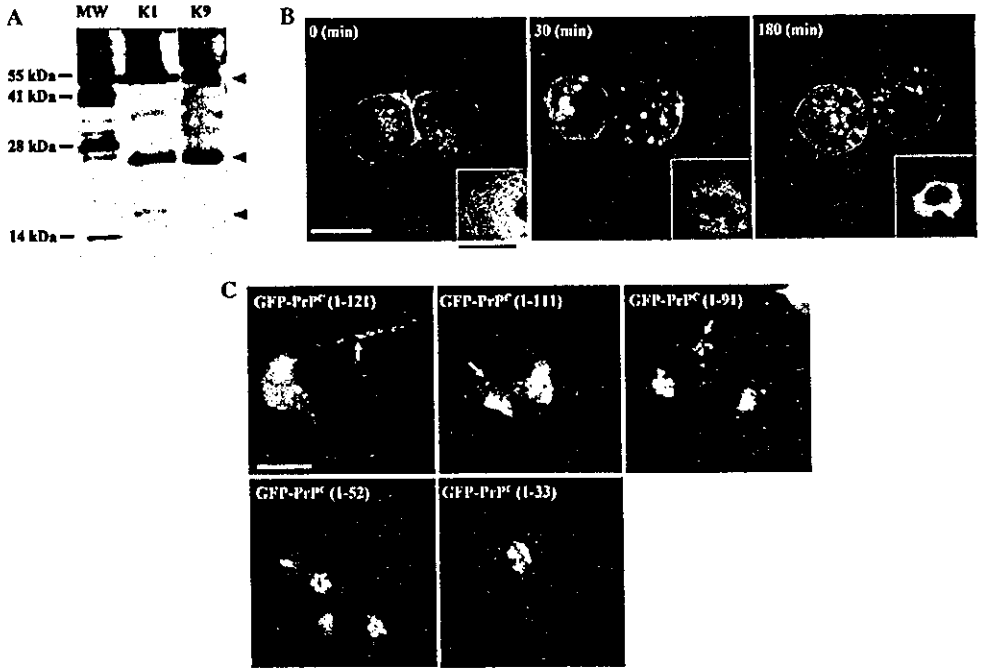


Fig. 3. The association of intracellular GFP–$PrP^C$ with microtubules. (A) Co-immunoprecipitation of tubulin and the $NH_2$-terminal $PrP^C$ fragment. Anti-tubulin antibody DM1A is used for the immunoprecipitation, and a polyclonal antibody K1 (1:500) against PrP residues 26–40 but not K9 (1:500) against residues 196–210 detects the $NH_2$-terminal $PrP^C$ fragment of 17 kDa (lower arrow head) in the immunoprecipitated complex. Both K1 and K9 detect full length $PrP^C$ (middle arrow head) and DM1A (1:2000) detects tubulin (upper arrow head). (B) After N2a cells were treated with 33 μM nocodazole and permeabilized with 0.1% Triton X-100, signals of GFP–$PrP^C$ congregate in a time-dependent manner (0–180 min). Panels at the lower right corners represent depolymerized microtubules stained with anti-tubulin antibody DM1A (1:200). Scale bars = 15 μm. (C) The truncated GFP–PrP constructs with the amino acid residues 1–121, 1–111, and 1–91 in Mo PrP exhibit its proper localization (arrows), whereas those with 1–52 and 1–33 lose its dot-like distribution pattern. Scale bar = 15 μm.

N-proximal domain of the PrP functions as a putative targeting element and is essential for both transport to the plasma membrane and modulation of endocytosis. Along with these observations, GFP-tagged version of $PrP^C$ was found to be properly anchored at the cell surface and its distribution pattern was similar to that of the endogenous $PrP^C$, with labeling at the plasma membrane and in an intracellular perinuclear compartment [10]. Further investigation concluded that $PrP^C$ internalizes via a dynamin-dependent endocytic pathway and that the protein is targeted to the recycling endosomal compartment via Rab5-positive early endosomes and thus, traffic of GFP–$PrP^C$ is delivered to classic endosomes after internalization [17]. Under our culture conditions, however, we could not demonstrate co-localization of the $NH_2$-terminal $PrP^C$ fragment with any single specific organelle so far examined.

With this background, we have shown the microtubules-dependent intracellular localization of the $NH_2$-terminal $PrP^C$ fragment in the cells. However, the question how intracellular $PrP^C$ actually interacts with microtubules still remains to be examined. After internalized, the $NH_2$-terminal $PrP^C$ fragment seems to reside inside vesicles where integral membrane proteins and linker proteins in some cases, for example, Jun kinase-interacting proteins (JIPs) [24,25], would be required for the interaction with microtubules to bridge the luminal and cytoplasmic phases across the membranes [26]. So far, we have not identified such intervening molecule/s involved in the $PrP^C$–microtubule interaction. Alternatively, a transmembrane form of $PrP^C$ may be engaged in the direct interaction with the microtubules. It was suggested that a transmembrane form of $PrP^C$, termed C-transmembrane ($^{ctm}PrP$), has the COOH-terminus in the lumen with the $NH_2$-terminus accessible to proteases in the cytosol produced neurodegenerative changes in mice similar to those of some genetic prion diseases [27]. Such $^{ctm}PrP$ exposes its $NH_2$-terminus to the cytosol where the $^{ctm}PrP$–microtubule interactions could theoretically occur, although it is less likely, as such transmembrane $^{ctm}PrP$ is rather pathogenic than physiologic. The fact that the truncated $PrP^C$ with residues 1–91 cannot form $^{ctm}PrP$ [27], but still exhibits the microtubules-associated intracellular localization, also does not support the notion. Interestingly, these residues 1–91 partly overlap with an octapeptide repeat region, which is related to the copper metabolism [28–32]. Finally, it is also indispensable for identifying how many $NH_2$-terminal $PrP^C$ fragments reside in each dot-like vesicle.

In summary, we demonstrated the microtubules-associated intracellular localization of $NH_2$-terminal $PrP^C$ fragment at a steady state level. At the same time, a real time imaging analysis of fluorescent $PrP^C$ in living cells has yet to be done toward further understanding of its mode of existence and dynamics along the microtubular network.

## Acknowledgments

We greatly thank S.B. Prusiner and D.A. Harris for discussions and comments, T. Onodera for providing us the HpL3-4 cell line, M. Kawabata, E. Nannri, C. Ota, and Y. Yamaura for technical assistances. This work was supported by grants from the Core Research for Evolutional Science and Technology (CREST) of Japan Science and Technology Agency, Health and Labour Sciences Research Grants, Research on Advanced Medical Technology, nano-001, and the Ministry of Health, Labor, and Welfare of Japan.

## References

[1] C. Kuwahara, A.M. Takeuchi, T. Nishimura, K. Haraguchi, A. Kubosaki, Y. Matsumoto, K. Saeki, T. Yokoyama, S. Itohara, T. Onodera, Prions prevent neuronal cell-line death, Nature 400 (1999) 225–226.
[2] S.B. Prusiner, Prions, Proc. Natl. Acad. Sci. USA 95 (1998) 13363–13383.
[3] S.B. Prusiner, D.C. Bolton, D.F. Groth, K.A. Bowman, S.P. Cochran, M.P. McKinley, Further purification and characterization of scrapie prions, Biochemistry 21 (1982) 6942–6950.
[4] S.B. Prusiner, P. Peters, K. Kaneko, A. Taraboulos, V. Lingappa, F.E. Cohen, S.J. DeArmond, Cell biology of prions, in: S.B. Prusiner (Ed.), Prion Biology and Diseases, Cold Spring Harbor, New York, 1999, pp. 349–391, Chap. 9.
[5] N. Stahl, D.R. Borchelt, K. Hsiao, S.B. Prusiner, Scrapie prion protein contains a phosphatidylinositol glycolipid, Cell 51 (1987) 229–240.
[6] B. Caughey, R.E. Race, D. Ernst, M.J. Buchmeier, B. Chesebro, Prion protein biosynthesis in scrapie-infected and uninfected neuroblastoma cells, J. Virol. 63 (1989) 175–181.
[7] A. Taraboulos, M. Scott, A. Semenov, D. Avrahami, L. Laszlo, S.B. Prusiner, Cholesterol depletion and modification of COOH-terminal targeting sequence of the prion protein inhibit formation of the scrapie isoform, J. Cell Biol. 129 (1995) 121–132.
[8] M. Vey, S. Pilkuhn, H. Wille, R. Nixon, S.J. DeArmond, E.J. Smart, R.G. Anderson, A. Taraboulos, S.B. Prusiner, Subcellular colocalization of the cellular and scrapie prion proteins in caveolae-like membranous domains, Proc. Natl. Acad. Sci. USA 93 (1996) 14945–14949.
[9] K. Kaneko, M. Vey, M. Scott, S. Pilkuhn, F.E. Cohen, S.B. Prusiner, COOH-terminal sequence of the cellular prion protein directs subcellular trafficking and controls conversion into the scrapie isoform, Proc. Natl. Acad. Sci. USA 94 (1997) 2333–2338.
[10] K.S. Lee, A.C. Magalhaes, S.M. Zanata, R.R. Brentani, V.R. Martins, M.A. Prado, Internalization of mammalian fluorescent cellular prion protein and N-terminal deletion mutants in living cells, J. Neurochem. 79 (2001) 79–87.
[11] L. Ivanova, S. Barmada, T. Kummer, D.A. Harris, Mutant prion proteins are partially retained in the endoplasmic reticulum, J. Biol. Chem. 276 (2001) 42409–42421.
[12] A. Negro, C. Ballarin, A. Bertoli, M.L. Massimino, M.C. Sorgato, The metabolism and imaging in live cells of the bovine prion protein in its native form or carrying single amino acid substitutions, Mol. Cell Neurosci. 17 (2001) 521–538.
[13] H. Lorenz, O. Windl, H.A. Kretzschmar, Cellular phenotyping of secretory and nuclear prion proteins associated with inherited prion diseases, J. Biol. Chem. 277 (2002) 8508–8516.
[14] D.A. Butler, M.A. Scott, J.M. Bockman, D.R. Borchelt, A. Taraboulos, K.K. Hsiao, D.T. Kingsbury, S.B. Prusiner, Scrapie-

infected murine neuroblastoma cells produce protease-resistant prion proteins, J. Virol. 62 (1988) 1558–1564.
[15] M.R. Scott, R. Kohler, D. Foster, S.B. Prusiner, Chimeric prion protein expression in cultured cells and transgenic mice, Protein Sci. 1 (1992) 986–997.
[16] T.A. Schroer, M.P. Sheetz, Role of kinesin and kinesin-associated proteins in organelle transport, in: F.D. Warner, J.R. McIntosh (Eds.), Cell Movement, Alan R. Liss, New York, 1989, pp. 295–306.
[17] A.C. Magalhaes, J.A. Silva, K.S. Lee, V.R. Martins, V.F. Prado, S.S.G. Ferguson, M.V. Gomez, R.R. Brentani, M.A.M. Prado, Endocytic intermediates involved with the intracellular trafficking of a fluorescent cellular prion protein, J. Biol. Chem. 277 (2002) 33311–33318.
[18] R.J. Kascsak, R. Rubenstein, P.A. Merz, M. Tonna-DeMasi, R. Fersko, R.I. Carp, H.M. Wisniewski, H. Diringer, Mouse polyclonal and monoclonal antibody to scrapie-associated fibril proteins, J. Virol. 61 (1987) 3688–3693.
[19] M. Rogers, D. Serban, T. Gyuris, M. Scott, T. Torchia, S.B. Prusiner, Epitope mapping of the Syrian hamster prion protein utilizing chimeric and mutant genes in a vaccinia virus expression system, J. Immunol. 147 (1991) 3568–3574.
[20] K.-M. Pan, N. Stahl, S.B. Prusiner, Purification and properties of the cellular prion protein from Syrian hamster brain, Protein Sci. 1 (1992) 1343–1352.
[21] S.-L. Shyng, J.E. Heuser, D.A. Harris, A glycolipid-anchored prion protein is endocytosed via clathrin-coated pits, J. Cell Biol. 125 (1994) 1239–1250.
[22] S.-L. Shyng, K.L. Moulder, A. Lesko, D.A. Harris, The N-terminal domain of a glycolipid-anchored prion protein is essential for its endocytosis via clathrin-coated pits, J. Biol. Chem. 270 (1995) 14793–14800.
[23] M. Nunziante, S. Gilch, H.M. Schatzl, Essential role of the prion protein N terminus in subcellular trafficking and half-life of cellular prion protein, J. Biol. Chem. 278 (2003) 3726–3734.
[24] A.B. Bowman, A. Kamal, B.W. Ritchings, A.V. Philp, M. McGrail, J.G. Gindhart, L.S. Goldstein, Kinesin-dependent axonal transport is mediated by the sunday driver (SYD) protein, Cell 103 (2000) 583–594.
[25] K.J. Verhey, D. Meyer, R. Deehan, J. Blenis, B.J. Schnapp, T.A. Rapoport, B. Margolis, Cargo of kinesin identified as JIP scaffolding proteins and associated signaling molecules, J. Cell Biol. 152 (2001) 959–970.
[26] M. Schliwa, G. Woehlke, Molecular motors, Nature 422 (2003) 759–765.
[27] R.S. Hegde, J.A. Mastrianni, M.R. Scott, K.A. DeFea, P. Tremblay, M. Torchia, S.J. DeArmond, S.B. Prusiner, V.R. Lingappa, A transmembrane form of the prion protein in neurodegenerative disease, Science 279 (1998) 827–834.
[28] D.R. Brown, K. Qin, J.W. Herms, A. Madlung, J. Manson, R. Strome, P.E. Fraser, T. Kruck, A. von Bohlen, W. Schulz-Schaeffer, A. Giese, D. Westaway, H. Kretzschmar, The cellular prion protein binds copper in vivo, Nature 390 (1997) 684–687.
[29] P.C. Pauly, D.A. Harris, Copper stimulates endocytosis of the prion protein, J. Biol. Chem. 273 (1998) 33107–33110.
[30] M.L. Kramer, H.D. Kratzin, B. Schmidt, A. Romer, O. Windl, S. Liemann, S. Hornemann, H. Kretzschmar, Prion protein binds copper within the physiological concentration range, J. Biol. Chem. 276 (2001) 16711–16719.
[31] W.S. Perera, N.M. Hooper, Ablation of the metal ion-induced endocytosis of the prion protein by disease-associated mutation of the octarepeat region, Curr. Biol. 11 (2001) 519–523.
[32] A.P. Garnett, J.H. Viles, Copper binding to the octarepeats of the prion protein. Affinity, specificity, folding, and cooperativity: insights from circular dichroism, J. Biol. Chem. 278 (2003) 6795–6802.
[33] N. Naslavsky, R. Stein, A. Yanai, G. Friedlander, A. Taraboulos, Characterization of detergent-insoluble complexes containing the cellular prion protein and its scrapie isoform, J. Biol. Chem. 272 (1997) 6324–6331.